

CFD Analysis of Flow Behavior in S-shape Air-Intake System of an Aircraft

By

SIDHARTHA SONDH

12MMET33



DEPARTMENT OF MECHANICAL ENGINEERING

INSTITUTE OF TECHNOLOGY

NIRMA UNIVERSITY

AHMEDABAD-382481

MAY 2014

CFD Analysis of Flow Behavior in S-shape Air-Intake System of an Aircraft

Major Project

Submitted in partial fulfillment of the requirements

For the Degree of

Master of Technology in Mechanical Engineering (Thermal Engineering)

By

Sidhartha Sondh (12MMET33)

Guide By

Prof A M Lakdawala

Mr. Irshad Khan



DEPARTMENT OF MECHANICAL ENGINEERING

AHMEDABAD-382481

MAY 2014

Declaration

This is to certify that

1. The thesis comprises my original work towards the degree of Master of Technology in Thermal Engineering at Nirma University and has not been submitted elsewhere for a degree.
2. Due acknowledgment has been made in the text to all other material used.

Sidhartha Sondh

12MMET33

Undertaking for Originality of the Work

I, Sidhartha Sondh, Roll. No. 12MMET33, give undertaking that the Major Project entitled “CFD Analysis of Flow Behavior in S-shape Air-Intake System of an Aircraft” submitted by me, towards the partial fulfillment of the requirements for the degree of Master of Technology in Mechanical Engineering (Thermal Engineering) of Nirma University, Ahmedabad, is the original work carried out by me and I give assurance that no attempt of plagiarism has been made. I understand that in the event of any similarity found subsequently with any published work or any dissertation work elsewhere; it will result in severe disciplinary action.

Signature of Student

Date: -----

Place: -----

Endorsed by

(Signature of Guide)

Certificate

This is to certify that the Major Project entitled “CFD Analysis of Flow Behavior in S-shape Air-Intake System of an Aircraft” submitted by Mr. Sidhartha Sondh (12MMET33), towards the partial fulfillment of the requirements for the of Degree of Master of Technology in Mechanical Engineering (Thermal Engineering) of Institute of Technology, Nirma University, Ahmadabad is the record of work carried out by him under our supervision and guidance. In our opinion, the submitted work has reached a level required for being accepted for examination. The result embodied in this major project, to the best of our knowledge, have not been submitted to any other University or Institution for award of any degree.

Mr. Irshad Khan
COO, Zeus Numerix,
Pune (Maharashtra).

Prof A M Lakdawala
Department of Mechanical Engineering,
Institute of Technology, Nirma University,
Ahmedabad.

Dr R N Patel
Head,
Department of Mechanical Engineering,
Institute of Technology, Nirma University,
Ahmedabad.

Dr K Kotecha
Director,
Institute of Technology,
Nirma University,
Ahmedabad.

Acknowledgments

First and foremost I would like to thank my institute guide Prof. A M Lakdawala and the industrial guide Mr. Irshad Khan for their continuous support, advice and encouragement during the course of this work.

I would also like to offer my sincere thanks and due respect to Dr R N Patel, (HOD, Department of Mechanical Engineering, IT, NU) and Dr K Kotecha (Director, IT, NU) who have directly or indirectly helped me during this dissertation work.

I am very much thankful to Mr. Vivek Warade and Mr. Sumit Jha and other staff of Zeus Numerix Prvt. Ltd. for their assistance and help in the thesis work.

I am thankful to all the faculty members of Mechanical Engineering Department for their expertise knowledge and guidance throughout my project work, which has provide me valuable insight in number of areas.

I thank all of my friends who were there for me all the time, during my course work and helped me when I needed them.

Finally I would like to express my gratitude to Nirma University and Zeus Numerix Pvt. Ltd., Pune (Maharashtra) for providing me excellent facilities and high performance computing resources and technical support for my project.

Sidhartha Sondh

12MMET33

Abstract

The project aims at investigating the flow behavior in an S-shape air-intake of an aircraft using the help of Computational Fluid Dynamics. S-shape air-intake is used in many aircraft like Boeing-727, Eurofighter Typhoon. In an S-duct, due to the change in the geometry at sections, there is origin of secondary flow which results in the total pressure drop. The variations in different flow parameters like static pressure, total pressure, Mach number along the duct length were studied. In this study, two cases are studied using a simple S-duct configuration and a modified S-duct configuration. The S-shape intake is modified by installing the guide vanes near the throat section of the duct. The angle of incidence is changed for the guide vanes from 0° , 8° and 16° . The modification in the duct is done to decrease the total pressure loss at the engine face and to improve the total pressure recovery. The two configurations were solved for different Mach numbers (0.4, 0.5, 0.6, 0.7, and 0.8) and two flight angle of attack 0° and 10° respectively. For the first configuration a structured grid is generated in GridZ where as for the second configuration an unstructured grid is generated in ICEM-CFD meshing software. To obtain the best results near the boundary of the intake, clustering operation was done for the Structured grid where as, a prism layer was generated for the same purpose in the T-Grid software. The computation of both the configurations was done in CFD-Expert-Lite solver. All the cases were run using Spalart Allmaras turbulence model.

Keyword: *S-shape air-intake, total pressure recovery, structured mesh, guide-vanes.*

List of Figures

3.1	S-shape air intake geometry	14
3.2	Vortex generator configuration	15
3.3	PBLS generated from NURB surface	17
3.4	2-D block generated for the geometry	18
3.5	Structured mesh with O-grid	18
3.6	Final grid after clustering	19
3.7	Unstructured mesh on S-shape air-intake	20
3.8	S-shape air-intake with boundary conditions	22
4.1	Different Grids: (a) Coarse grid, (b) Normal grid, (c) Fine grid, (d) Finest grid	24
4.2	$L - 1$ and $L - 2$ norm grid convergence	25
4.3	Axi-symmetric Total Pressure profile: (a) at 0^0 Angle of Attack (AoA) for Mach number 0.8, (b) at 0^0 AoA for Mach number 0.7, (c) at 0^0 AoA for Mach number 0.6, (d) at 0^0 AoA for Mach number 0.5, (e) at 10^0 AoA for Mach number 0.8, (f) at 10^0 AoA for Mach number 0.8, (g) at 10^0 AoA for Mach number 0.7, (h) at 10^0 AoA for Mach number 0.6, (i) at 10^0 AoA for Mach number 0.5, (j) at 10^0 AoA for Mach number 0.4.	26
4.4	Axi-symmetric Mach number profile: (a) at 0^0 Angle of Attack (AOA) for Mach number 0.8 (b) at 0^0 AoA for Mach number 0.7, (c) at 0^0 AoA for Mach number 0.6, (d) at 0^0 AoA for Mach number 0.5, (e) at 10^0 AoA for Mach number 0.8, (f) at 10^0 AoA for Mach number 0.8, (g) at 10^0 AoA for Mach number 0.7, (h) at 10^0 AoA for Mach number 0.6, (i) at 10^0 AoA for Mach number 0.5, (j) at 10^0 AoA for Mach number 0.4.	28
4.5	Total Pressure Recovery Plot	30

4.6	Total Pressure recovery at AIP or engine face for: (a) 0^0 AoA and 0.8 Mach number, (b) 0^0 AoA and 0.7 Mach number, (c) 0^0 AoA and 0.6 Mach number, (d) 0^0 AoA and 0.5 Mach number, (e) 10^0 AoA and 0.8 Mach number, (f) 10^0 AoA and 0.7 Mach number, (g) 10^0 AoA and 0.6 Mach number, (h) 10^0 AoA and 0.5 Mach number, (i) 10^0 AoA and 0.5 Mach number.	31
4.7	Axi-symmetric Total Pressure profile: (a) for 10^0 intake AoA and 16^0 vane effector angle for 0.8 Mach number, (b) for 10^0 intake AoA and 16^0 vane effector angle for 0.7 Mach number, (c) for 10^0 intake AoA and 8^0 vane effector angle for 0.8 Mach number, (d) for 10^0 intake AoA and 8^0 vane effector angle for 0.7 Mach number, (e) for 10^0 intake AoA and 0^0 vane effector angle for 0.8 mach, (f) for 10^0 intake AoA and 0^0 vane effector for 0.7 mach.	33
4.8	Axi-symmetric Mach Number profile: (a) for 10^0 intake AoA and 16^0 vane effector angle for 0.8 Mach number, (b) for 10^0 intake AoA and 16^0 vane effector angle for 0.7 Mach number, (c) for 10^0 intake AoA and 8^0 vane effector angle for 0.8 Mach number, (d) for 10^0 intake AoA and 8^0 vane effector angle for 0.7 Mach number, (e) for 10^0 intake AoA and 0^0 vane effector angle for 0.8 mach, (f) for 10^0 intake AoA and 0^0 vane effector for 0.7 mach.	34
4.9	Total Pressure Recovery with vane-effectors at different angles for 10^0 AoA .	35
A.1	Axi-symmetric profile of Static pressure variation for (a) Mach number 0.8 at 0^0 AoA, (b) Mach number 0.7 at 0^0 AoA, (c) Mach number 0.6 at 0^0 AoA, (d) Mach number 0.5 at 0^0 AoA, (e) Mach number 0.8 at 10^0 AoA, (f) Mach number 0.7 at 10^0 AoA, (g) Mach number 0.6 at 10^0 AoA, (h) Mach number 0.5 at 10^0 AoA	40
A.2	Axi-symmetric profile of Density variation for (a) Mach number 0.8 at 0^0 AoA, (b) Mach number 0.7 at 0^0 AoA, (c) Mach number 0.6 at 0^0 AoA, (d) Mach number 0.5 at 0^0 AoA, (e) Mach number 0.8 at 10^0 AoA, (f) Mach number 0.7 at 10^0 AoA, (g) Mach number 0.6 at 10^0 AoA, (h) Mach number 0.5 at 10^0 AoA	41
B.1	Axi-symmetric Static Pressure variation profile for 10^0 AoA (a) Mach number 0.8 at 16^0 angle of incidence of vane effector, (b) Mach number 0.7 at 16^0 angle of incidence of vane effector, (c) Mach number 0.8 at 8^0 angle of incidence of vane effector, (d) Mach number 0.7 at 8^0 angle of incidence of vane effector, (e) Mach number 0.8 at 0^0 angle of incidence of vane effector, (f) Mach number 0.7 at 0^0 angle of incidence of vane effector.	42

B.2 Axi-symmetric Density variation profile for 10° AoA (a) Mach number 0.8 at 16° angle of incidence of vane effector, (b) Mach number 0.7 at 16° angle of incidence of vane effector, (c) Mach number 0.8 at 8° angle of incidence of vane effector, (d) Mach number 0.7 at 8° angle of incidence of vane effector, (e) Mach number 0.8 at 0° angle of incidence of vane effector, (f) Mach number 0.7 at 0° angle of incidence of vane effector. 43

List of Tables

4.1	Initial Conditions used for the solutions	23
4.2	Values of Total Pressure Recovery obtained for 0^0 and 10^0 AoA	29
4.3	Total Pressure Recovery for different vane-effector configurations	35

Nomenclature

P_i	Total Pressure at inlet
P_f	Total Pressure at outlet
ΔP	Pressure Difference
q	Dynamic Pressure
PR	Pressure Recovery
R_{th}	Radius of the throat
R_{ef}	Radius of the engine face
L	Length of the air-intake
ΔZ_{cl}	Center line duct offset
P_N	Total Pressure at the face
P_{avg}	Average Freestream Total Pressure
N	Number of grid points on the face

Greek Symbol

α	Angle of Attack
ν	kinematic viscosity of the fluid [= m^2/s]
ρ	Density of the fluid [= kg/m^3]

Abbreviation

S-duct	Serpentine duct
Pa	Pascals
UAV	Unmanned Air Vehicle
CFD	Computational Fluid Dynamics
ZNMF	Zero- Net Mass flow
PIV	Particle Investigation Velocimetry
SA	Spalart Allmaras Model
SST	Shear Stress Transport
NSE	Navier Stokes Equation
RANS	Reynolds Averaged Navier Stokes Equation
TPR	Total Pressure Recovery
NURBS	Non-uniform Rational B-Spline
PBLS	Piecewise Bilinear Surface
PLC	Piecewise Linear Curve

Contents

Declaration	iii
Undertaking for Originality of the Work	iv
Certificate	v
Acknowledgments	vi
Abstract	vii
List of Figures	viii
List of Table	xi
Nomenclature	xii
Contents	xiv
1 Introduction	1
1.1 Computational Fluid Dynamics	2
1.2 Flow Physics inside the S-shape Air-intake	3
1.3 Definition of Problem	3
1.4 Motivation	3
1.5 Objective	4
1.6 Outline of Report	4
2 Literature Review	6
2.1 Experimental Research	6
2.2 Numerical Research	7
2.3 Numerical and Experimental Work	8
2.4 Conclusion from Literature Review	9

3	Mathematical Modeling and Numerical Techniques	10
3.1	Governing Equation	11
3.1.1	Continuity equation:	11
3.1.2	Momentum Equation:	11
3.2	Important Parameters	12
3.3	Modeling of S-shape air-intake	13
3.4	Mesh generation	15
3.4.1	Blocking	16
3.4.2	O-grid	16
3.4.3	Procedure for Structured mesh generation	16
3.4.4	Unstructured Mesh	19
3.5	Computational Procedure in CFD-ExpertLite	20
3.5.1	Discretization method	21
3.5.2	Boundary Conditions	21
3.5.3	Initial Conditions	22
4	Results and Discussions	23
4.1	Initial Conditions	23
4.2	Grid Independent Study	24
4.2.1	Grid Convergence criteria	24
4.3	Results obtained	25
4.3.1	S-shape air intake without vane-effectors	25
4.3.2	Total Pressure Recovery	28
4.3.3	S-shape air-intake with vane-effectors	31
4.3.4	Total Pressure Recovery	34
5	Conclusion and Future Scope	36
5.1	Conclusion	36
5.2	Future Scope	37
	Bibliography	38
	Appendix	39
A	Flow inside an S-shape air-intake without Vane-effectors	40
B	Flow inside an S-shape intake with Vane effectors	42

Chapter 1

Introduction

The objective of this chapter is to basic introduction of compressible, subsonic flow inside an S-shape air-intake. The various types of the flow disturbance that occurs in the air-intake are discussed. The chapter also defines the problem that is studied, the objective of the project as well as the outline of the report is also given.

Flow in curved ducts are found in a wide range of practical configurations. The most frequently used are S-shaped ducts and passages which occurs in a number of applications, where a combinations of bends are employed to redirect the flow. The S-duct finds a vast importance role in the aerospace industry as well. This S-duct is usually a mean of conveying air from fuselage or wing intake to the engine compressor. In such applications compressible, subsonic flow condition exists. The internal flow is one of the most complex type of flows to visualize as well as to analyze.

Some of the commercial aircraft with S-ducts are Boeing 727, Lockheed Tristar, Dassault Falcon 900. Amongst the military aircraft include Eurofighter Typhoon, F16. Due to the curving nature and changing cross-section of the S-duct, there is an origin of secondary flows and boundary layer separation at the downstream bends of the duct. These effects cause the flow to become non-uniform and also increase the total pressure loss at the engine face. Since there is always a necessity to minimize size and maximize stealth of aircraft, including Unmanned Air Vehicles (UAVs), designers are challenged to use shorter and more highly curved S-ducts. S-ducts maximize the stealth characteristics of the aircraft by hiding the spinning turbine blades which reflect radar. If the length of the S-duct is shortened, the curvature of the duct increases rapidly and therefore there is a rise in adverse pressure

gradients and secondary flow. Thus this leads to a drop in the performance.

It is often seen that the cross-sectional area of the S-shape air-intake increases gradually as it goes to the downstream of the intake. This is done in order to decelerate the flow and achieve a higher static pressure at the intake outlet or the engine face. To achieve the maximum engine performance, the air-intake should minimize the pressure losses that occurs at the bend section and the flow separation that occurs at the downstream of the bend. If the changes are made in the cross-section and curvature of the intake center line then there is a origin of secondary flow due to the rise in streamline curvature. Also, the cross streamline pressure gradients that results from the streamline curvature can lead to flow separation. The size and weight restriction in aerospace industry often encourages the use of shorter S-shape air-intake. This results in greater streamline curvature and results in adverse pressure gradient. This results in increasing the risk of unacceptable intake performance.

The fluid flow can be analyzed by two approach. the approaches being experimental and numerical. In the experimental approach, a real model is made whereas an experimental setup is also made. The testing of the model is done in the wind tunnel by applying the flow conditions. The results are calculated by installing the devices such as pressure transducers to record the readings at different locations of the model. The other approach that is used is numerical. In this method the results are obtained by solving equations. These equations are usually very complex and hectic to be solved. For the numerical approach, a numerical model of the specimen is made. The theoretical results are generated by solving the numerical model for certain flow conditions.

1.1 Computational Fluid Dynamics

Gas dynamics is a branch of fluid dynamics, concerned with the study of motion of gases and its effect on physical systems. Gas dynamics works on the principle of fluid mechanics and thermodynamics. Gas dynamics theories are majorly used in in aerospace industry. The flow of gas is in transonic and supersonic flows. Frictional forces play a role in determining the flow properties of compressible flows in ducts. Computational fluid dynamics analysis provides an insight to the flow pattern and it also helps identifying the unfavorable flow regions. The origin of separated flow gives rise to pressure fluctuation on the duct surface. CFD can be used for analyzing the flow in ducts in order to provide the flow distribution, pressure loss for the complete system.

Computational Fluid Dynamic is field of science and engineering which is rapidly growing due to the development in the mathematical methods and computing resources. CFD is a mathematical model of Fluid Dynamics which takes conservations equations, convert the

equation into algebraic equations. These algebraic equations are solvable with the help of mathematical techniques.

The recent development in the mathematical techniques and availability of super computing has made CFD a reliable source for the research study.

1.2 Flow Physics inside the S-shape Air-intake

As we know, S-shape air-intake is a curved duct. The curved geometry of the duct causes the flow inside the duct to be complex. The function of the S-duct is to decelerate the flow, to increase the static pressure, in order to provide a uniform velocity and pressure distribution at the engine face. An ideal S-shape air-intake completely verifies this theory by producing uniform velocity and pressure distribution at the engine face. An ideal S-shape air-intake efficiently decelerates the flow while minimizing the total pressure loss and reducing the magnitude of transverse velocity component. But in a real case this is not achieved. The flow is uniform till the first bend of the duct. As the flow progresses downstream of the bend, the flow tends to break. This is due to the rise of the eddies at that bend section of the duct. These eddies are in form of flow separation and secondary flows.

Due to this disturbance in flow there is a huge pressure drop at the bend section of the duct, that accounts for overall drop in total pressure recovery at the engine face. The drop in the total pressure recovery is directly related as the drop in air-intake efficiency, as the engine utilizes the total pressure recovery by intake for generating the thrust.

1.3 Definition of Problem

In this project a numerical study of flow inside an S-shape air-intake is done. The effect of flow separation and pressure drop at different section on the total pressure recovery at engine face is studied. The performance of the intake is improved by installing the guide vanes that works as a vortex generator. All the cases were run for a mach number ranging from 0.4-0.8 and for two angle of attacks 0° and 10° . The geometry is made using ICEM-CFD-14.5 and analysis was carried out using CFD-ExpertLite.

1.4 Motivation

CFD is widely used in aerospace industry as an analysis tool to test and validate the design of the aircraft parts and whole system. There are constantly questions asked on the accuracy of the solution achieved because it depends on the accuracy of the algorithm, type and quality

of the mesh, solver, turbulence model. There are several configuration that have highly 3-D flows which can give rise to a very complex flow phenomena posing a challenge for CFD software. One such configuration is S-shape air-intake.

The flow inside the S-duct is characterized by boundary layer separation and secondary flow duct to the curved shape. The rise in total pressure loss and non-uniformity of the flow at the engine face causes the engine performance to drop. The engine performance drops because it does not get enough air pressure to generate the required thrust force.

1.5 Objective

The main objective of the present study is to analyze the flow behavior inside an S-shape air-intake. The objectives of the project can be listed as:

- Initially, a grid independent study was carried out for the S-shape air-intake at 0.6 mach and zero angle of attack. Also the result obtained are compared with available literature result to validate methodology.
- The flow inside an S-duct was analyzed for five mach number from 0.4-0.8 and two angle of attack 0° and 10° .
- For the 10° angle of attack case, a geometrical modification was also done. Here a vortex generator configuration was installed just after the throat where the pressure losses were occurring.
- The vortex generator blade's angle was also changed. This was studied for three angles 0° , 8° and 16° to analyze how this affects the total pressure recovery at the engine face.

1.6 Outline of Report

The outline of report is as follows:

Introduction about the project is given in chapter-1 which includes Flow Physics inside the S-shape Air-intake, Objective and Organization of Report. A brief introduction of the work carried out in the project is also given. Chapter-2 is named Literature Review, it contains History and Literature Review. All the numerical aspect of the project such as the governing equation to be solved, the type of grid chosen and the methodology to generate it in GridZ and ICEM-CFD-14.5 is discussed in chapter-3 of the report. This chapter also emphasizes on application of boundary condition, initial conditions, the numerical scheme

used for solution of the problem. Result and discussion which include quantitative results as well as the qualitative results are discussed in chapter-4. Chapter-5 explains Conclusion.

Chapter 2

Literature Review

The S-shape air-intake has been of huge interest to the researchers and therefore a number of researches have been carried out on a number of topics related to the S-shape air-inlet. The researchers have performed experimental research as well as numerical research on the S-shape air-intake. Different researchers used different techniques such as Zero-Net-Mass-Flow (ZNMF) jets to calculate different parameter such as swirl, distortion, total pressure recovery.

Flow inside an S-shape air-intake is one of the problem that provides the researchers with a challenge to solve a complex flow that is hindered by flow separation and secondary flows. The S-shape air-intake is an important part of aircraft. The factor of safety for the aerospace industry is very high so the researches done on these components need to be very accurate and efficient.

In this part of the report, the previously published researches are discussed. These researches can be categorized into (a) Experimental research (b) Numerical research and (c) Both Experimental and Numerical research.

2.1 Experimental Research

The flow characteristics as well as performance characteristics of an S-shape diffusing duct was investigated experimentally by Anand et al. (2008). The specification of the ducts were area-ratio 1.9, length 300mm, and turning angle $22.5^{\circ}/22.5^{\circ}$. The performance parameters were calculated based on mass averaged quantity. The experiment was setup in two phases,

in the first phase, the experiment was conducted with uniform flow at inlet and in the second phase, experiments were conducted for swirl flow. The experiments were carried at a mean axial velocity of 27 m/s at the inlet.

In a research carried out by Mathis et al. (2007), the investigation of flow was done using Zero -Net-Mass-Flow (ZNMF) in a two dimensional model of an S-shape air-intake diffuser. The experiments were conducted at a centreline velocity of $U_c = 12.4$ m/s and a Reynolds Number of 8×10^4 . Particle Investigation Velocimetry (PIV) measurements were performed in this investigation to capture the velocity field. A linear local stability analysis was also performed for the mean velocity field. The equation that governs the stability of a fluid system is the perturbation form of the Navier-Stokes Equations. It explains about the effect that small perturbations have on the transition to turbulence.

A research was carried out that aimed at experimental study of aerodynamic characteristics of a ventral divert less high offset S-shaped inlet at transonic speeds. Wenzhong et al. (2008), carried out this investigation on the ventral divert less high offset S-shaped inlet having a range of Mach numbers from 0.600 to 1.534, angle of attack from -4° to 9.4° , and yaw angles from 0° to 8° . In this research the static pressure coefficient distribution along the walls and total pressure recovery contours at the engine face. The experiments were carried out at NH-1 high speed wind tunnel at Nanjing University of Aeronautics.

2.2 Numerical Research

The flow in a diffusing S-shaped air-intake using the computational fluid dynamics simulation was examined by Menzies (2001). The model of S-duct used was RAE M-2129. The multi block structured grid was generated for the geometry. The grid was generated using ICM CFD software. For the better flow capture an O-type grid was generated for the intake and H-grid was generated for the large far field. The flow solver used for the calculation was the University of Glasgow's three dimensional flow solver named PMB3D. A cell centered finite volume technique was used. The turbulence model being used was Spalart -Allmaras (S-A), $k-\varepsilon$, Shear Stress Transport (SST) model.

A computational study of center line turning angle effect on the turbulent flow through a diffusing S-duct was performed by Abdellatif et al. The geometrical specification of the S-duct were $L/D = 11.4$, area ratio 1.9, centreline length of 600mm. A number of duct turning angle cases were studied, the angles being 15/15, 22.5/22.5 and 30/30. The simulations were performed at $Re = 10^5$ and at inlet velocity of 27 m/s. The velocity, total pressure and turbulence intensity distribution were calculated and compared with available experimental data. The turbulence model used was Large Eddy Simulations (LES) and $k-\varepsilon$ model. An

O-type structured grid was generated.

A numerical simulation of separated and secondary flow in diffusing S-ducts for air breathing propulsion was performed by Fiola (2013). The main aim of the project was to perform numerical simulations of incompressible and compressible flows in a diffusing S-duct inlet. Two S-duct geometries were employed in the investigation - one was used in experimental study conducted at NASA Glenn Research Center in the early 1990's, the other was the benchmark configuration proposed by AIAA Propulsion Aerodynamic Workshop to assess the accuracy and best practices of CFD services. A structured mesh was generated using GAMBIT. For the computational purpose solver Ansys FLUENT is employed. The turbulence model used was $k-\omega$, $k-\varepsilon$, Spalart-Allmaras and SST model.

Usually all the researchers used to analyze flow in a circular S-duct, but Singh et al. (2009), analyzed the performance characteristics of S-shaped rectangular diffuser by momentum injection using computational fluid dynamics. The geometrical specifications were area ratio = 2, angle of turn 90/90. The important performance parameters to be evaluated were created using GAMBIT modeling software. The geometry model was then meshed. Near the wall, boundary layer meshing was used to take care of steep velocity gradients and the rest of the part was meshed using hexahedral map meshing scheme. The analysis was carried out using the CFD code FLUENT 6.1.

The study of swirling flow in F-5E intake at different angle of attacks (AoA's) and angle of side slips (AoSS's) at subsonic speeds was carried out by Wu et al (2008). The concept of swirl, and the possibility of compressor stall and engine surge have also been studied. The parameters that were emphasized on were pressure recovery, distortion coefficient and swirl coefficient. The inlet cross-section was rectangular whereas outlet section is circular.

The modeling of the geometry was done using computer aided design program Pro/Engineer Wildfire 2.0. The meshing was done in GAMBIT 2.2. For the solver purpose FLUENT 6.2 was used. SST model is used as turbulence model.

2.3 Numerical and Experimental Work

The flow in a S-shape air-intake was studied using both experimental and numerical approach by Abrahamsen et al.(1998). Both the experimental and computational results were compared with AGARD working group 13s measurements of the RAE M-2129 S-duct. The effect of turbulence was accounted by the variations of commonly used model $k-\varepsilon$ model. The method employed for the time stepping was the second order 3 stage Runge Kutta method. The type of meshing done was the boundary fitted mesh. The experiment was performed using Isentropic Light Piston Tunnel facility. The parameters that were calculated from the

experiment were pressure recovery and static distortion parameter.

Compressible flow through a diffusing S-duct was investigated both experimentally as well as numerically by two researchers Wellborn and Okiishi (1993). The main parameters measured were three dimensional velocity field, total pressure and static pressure at different section plane. All the experiments were performed at NASA Lewis Research Center in the Internal Fluid Mechanics facility. The facility was designed to support test of a variety of internal flow configuration. the test section consisted of diffusing S-duct and two constant area extension. The flow field during the experiment was investigated by several different techniques for example flow visualization and wall static pressures.

The mathematical model used for the computational study was Parabolised Navier-Stokes Equation (PNSE). The code used for solving the flow was the PEPSIG. The grid distribution was done using algebraic grid generator. An O-grid was implemented in the cross-stream plane. The tests were conducted for Mach number 0.6, Reynolds number being 2.6×10^6 .

A numerical analysis of flow development through a constant area duct along with experimental work was investigated by Biswas et al (2012). The experimental work was carried on with measurement of mean velocity contours in 2-D form. The experimental results obtained were validated by numerical results based on y^+ approach at fully developed flow. The experiments were performed at the Aerodynamic Laboratory of National Institute of Technology Durgapur. The wind tunnel testing was performed for the protocol. The mass averaged mean velocity was 40 m/s. The researchers used a rectangular 90° curved duct of width 50mm and height of 100mm. GAMBIT was used to create the geometry, problem defining and for discretizing the domain. For the analysis purpose FLUENT 6.9 was used.

2.4 Conclusion from Literature Review

From the previous researches it could be concluded that the flow in the S-shape air-intake is hindered by a variety of eddies. Many phenomena like flow separation, rise of secondary flows, pressure losses, swirl flow all exists in this. The important parameters that tells the performance of the air-intake is distribution of the total pressure and velocity at the engine face. An account has to be kept for the pressure losses that occur at the bend of the S-duct. From the literature review few remedies to encounter this effect are known like the use of vortex generator.

In the present research the flow inside the s-duct is studied and along with it the the geometrical modification is done to encounter the eddies caused.

Chapter 3

Mathematical Modeling and Numerical Techniques

The objective of this chapter is to provide the information about the project's numerical aspects such as the governing equation, the boundary and initial conditions applied to solve the problem. The software used for the analysis part is CFD-Expertlite. The procedure that was followed throughout the procedure i.e., from modeling of the geometry, meshing, application of boundary conditions are all explained in this chapter. The basic aim of this project is to provide the knowledge of how to build the problem for the solution purpose.

Consider a steady, three dimensional viscous compressible flow inside a S-shape air-intake. The inlet of the air-intake was applied with the Pressure-Inflow boundary condition, whereas the outlet of the duct is provided with the Outflow boundary condition and the wall of the intake is given the Viscous wall boundary condition. For the second part of the problem where the geometrical modifications are done, the guide vanes are also given the Viscous wall boundary conditions. The vortex generator configuration was located just after the throat area where the problem area is situated. A straight constant area section of 340 mm is added at the upstream end of the duct in order to allow the code to develop a boundary layer. At the duct exit, a straight constant area section of 170 mm is added to push the boundary layer aft of the engine.

3.1 Governing Equation

The computation software that is used for analyzing the flow works by solving certain equations. This equation is known as governing equation. For the present study, the software chosen for the computation part is CFD-ExpertLite. Any CFD problem is governed by two equations namely, Continuity equation and Momentum equation. These equations when combined are known as Navier-Stokes Equations (NSE). Navier-Stokes Equation can be simplified to simplified forms according to the flow. For the present study time averaged NSE is studied. The time averaged NSE for a compressible flow can be defined as :

3.1.1 Continuity equation:

$$\frac{\partial \rho \bar{u}}{\partial x} + \frac{\partial \rho \bar{v}}{\partial y} + \frac{\partial \rho \bar{w}}{\partial z} = 0 \quad (3.1)$$

3.1.2 Momentum Equation:

X-direction

$$\begin{aligned} \frac{\partial \rho \bar{u}}{\partial t} + \bar{u} \frac{\partial \rho \bar{u}}{\partial x} + \bar{v} \frac{\partial \rho \bar{u}}{\partial y} + \bar{w} \frac{\partial \rho \bar{u}}{\partial z} = & -\frac{\partial P}{\partial x} + \mu \left(\frac{\partial^2 \bar{u}}{\partial x^2} + \frac{\partial^2 \bar{u}}{\partial y^2} + \frac{\partial^2 \bar{u}}{\partial z^2} \right) \\ & - \left(\frac{\partial \rho \overline{u'u'}}{\partial x} + \frac{\partial \rho \overline{u'v'}}{\partial y} + \frac{\partial \rho \overline{u'w'}}{\partial z} \right) + S_x \end{aligned} \quad (3.2)$$

Y-direction

$$\begin{aligned} \frac{\partial \rho \bar{v}}{\partial t} + \bar{u} \frac{\partial \rho \bar{v}}{\partial x} + \bar{v} \frac{\partial \rho \bar{v}}{\partial y} + \bar{w} \frac{\partial \rho \bar{v}}{\partial z} = & -\frac{\partial P}{\partial y} + \mu \left(\frac{\partial^2 \bar{v}}{\partial x^2} + \frac{\partial^2 \bar{v}}{\partial y^2} + \frac{\partial^2 \bar{v}}{\partial z^2} \right) \\ & - \left(\frac{\partial \rho \overline{v'u'}}{\partial x} + \frac{\partial \rho \overline{v'v'}}{\partial y} + \frac{\partial \rho \overline{v'w'}}{\partial z} \right) + S_y \end{aligned} \quad (3.3)$$

Z-direction

$$\begin{aligned} \frac{\partial \rho \bar{w}}{\partial t} + \bar{u} \frac{\partial \rho \bar{w}}{\partial x} + \bar{v} \frac{\partial \rho \bar{w}}{\partial y} + \bar{w} \frac{\partial \rho \bar{w}}{\partial z} = & -\frac{\partial P}{\partial z} + \mu \left(\frac{\partial^2 \bar{w}}{\partial x^2} + \frac{\partial^2 \bar{w}}{\partial y^2} + \frac{\partial^2 \bar{w}}{\partial z^2} \right) \\ & - \left(\frac{\partial \rho \overline{w'u'}}{\partial x} + \frac{\partial \rho \overline{w'v'}}{\partial y} + \frac{\partial \rho \overline{w'w'}}{\partial z} \right) + S_z \end{aligned} \quad (3.4)$$

Here \bar{u} \bar{v} and \bar{w} denotes the time averaged terms of velocity and u',v' and w' denotes

the fluctuating terms. The terms $\overline{\rho u' u'}$, $\overline{\rho u' v'}$ and $\overline{\rho u' w'}$ refers to the Reynolds Stresses in x direction. These are the source of turbulence in the flow. Similarly, the terms $\overline{\rho v' u'}$, $\overline{\rho v' v'}$, $\overline{\rho v' w'}$ and $\overline{\rho w' u'}$, $\overline{\rho w' v'}$, $\overline{\rho w' w'}$ are the Reynolds Stresses in y and z direction. It can be clearly seen that the number of unknowns in the equation are more than the number of equations. Therefore, some more equations are required that can solve these unknown parameters. These unknowns are solved by turbulence model. The turbulence model chosen for the present study is Spalart Allmaras turbulence model.

3.2 Important Parameters

In general, any duct has its own specific friction and loss. The pressure loss is defined as the ratio of pressure difference through the duct (i.e. the difference of pressure between inlet and outlet) to the dynamic pressure.

$$Pressure\ Loss = \frac{\Delta P}{q} = \frac{P_i - P_f}{q} \quad (3.5)$$

Here P_f is the mean total pressure at the outlet of the intake or engine face, P_i is the total pressure at the inlet and q is the dynamic pressure.

The most commonly used parameter to define the efficiency of the intake is the ratio of mean total pressure at the engine face to the free stream total pressure.

$$PR = \frac{P_{t2}}{P_{t\infty}} \quad (3.6)$$

where TPR is the total pressure recovery, P_{t2} is the mean total pressure at the intake's outlet and $P_{t\infty}$ is the free stream total pressure. In other words it could be said that,

$$Total\ Pressure\ Recovery = 1 - Total\ Pressure\ Loss \quad (3.7)$$

The total pressure through the inlet changes because of several flow effects. The aerodynamicists characterize the inlet's pressure performance by the inlet total pressure recovery, which measures the amount of the free stream flow conditions that are recovered. It is a

significant design parameter as a loss in total pressure is directly related to the loss in the engine thrust.

The pressure recovery factor depend on the number of factors, including the shape of the inlet, the speed of the aircraft, and the airflow demands of the engine and aircraft maneuvers. Therefore, a good inlet should produce a high pressure recovery. The maximum allowable pressure loss of an air-intake is reported smaller than 0.02 in many sources. A well designed air-intake should have a total pressure recovery of 0.98 or more.

As discussed earlier, one of the main tasks of the air-inlet is to deliver air uniformly to the compressor blades. This uniformity consists of total pressure, static pressure, total temperature, or a combination of above mentioned parameters.

3.3 Modeling of S-shape air-intake

The modeling of the S-shape air-intake was done using ICEM-CFD14.5. The specification of the duct were as follows: the radius of the throat of the intake, $R_{th} = 64.4\text{mm}$, the radius of the intake at the outlet of the intake or at the engine face, $R_{ef} = 76.2\text{mm}$. The distance between the throat section and the engine face, $L = 490\text{ mm}$. The inlet of the throat section is located 170 mm from the throat section. The overall length of the duct is 660 mm. The center line duct offset, $\Delta Z_{cl} = 68.58\text{ mm}$. The area of the duct increases gradually from the throat to the engine face. The outlet to inlet area ratio of the intake is 1.4. The center line radius of the duct was found by the formula mentioned below

$$Z_{cl} = -\Delta Z_{cl} \left[1 - \cos\left(\pi \times \frac{x_{cl}}{L}\right) \right] \quad (3.8)$$

$$\frac{R_{cl} - R_{th}}{R_{ef} - R_{th}} = \left[3\left(1 - \frac{x_{cl}}{L}\right)^4 - 4\left(1 - \frac{x_{cl}}{L}\right)^3 + 1 \right] \quad (3.9)$$

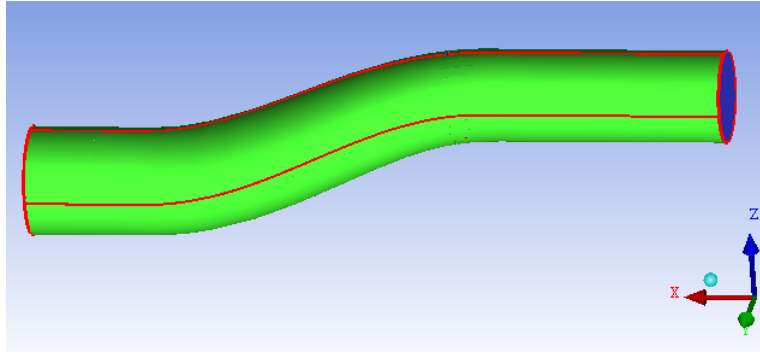
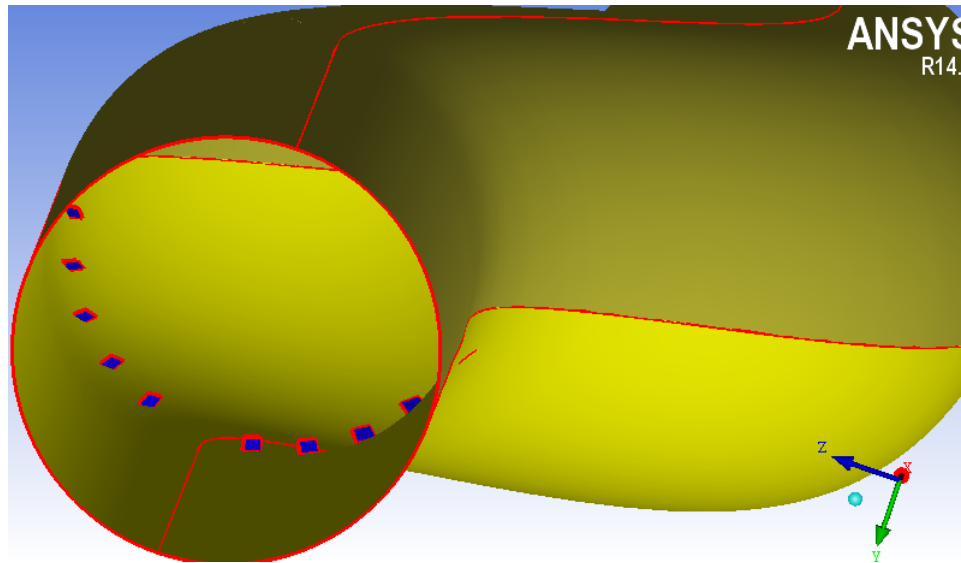
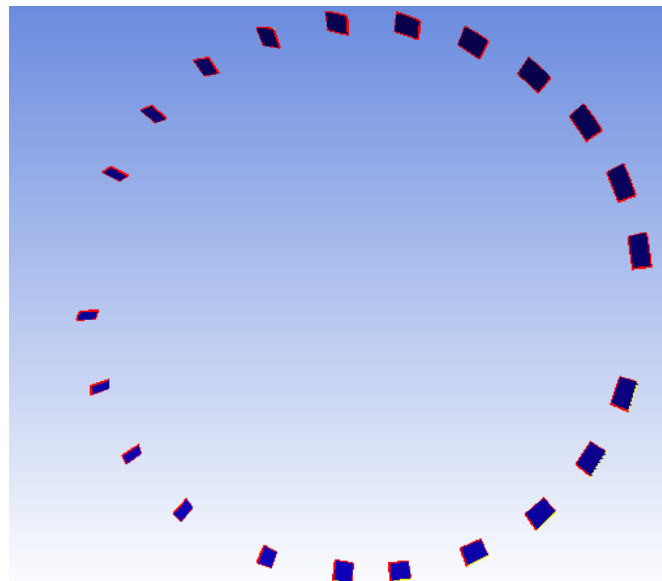


Figure 3.1: S-shape air intake geometry

For the second part of the project a vortex generator configuration was modeled. The vortex generator here are the guide-vanes that work in such a manner that it performs the function of vortex generator. The configuration of vane-effector is shown in Fig.3.2a, Fig.3.2b. A total of 22 guide-vanes were made. The vane-effectors were distributed around 157.5° sector per half duct. The vortex generator configuration contained 11 guide vanes in half duct. Each guide vane was spaced at an angle of 15 degree from the preceding guide-vane. Each vane-effector was a flat plate of aspect ratio 0.25 (height/chord) where the chord was approximately 17.78 mm.



(a) Vane effectors location



(b) The configuration of the vane effector working as vortex generator

Figure 3.2: Vortex generator configuration

3.4 Mesh generation

Mesh generation is a practice of generating a grid that approximates the geometric domain. The three dimensional meshes created for finite element analysis needs to be consist of tetrahedra, pyramids, prism or hexahedra. This shape of the mesh element depends upon the type of mesh that is chosen. Quadrilateral and hexahedral are for the structured mesh whereas the triangle and tetrahedral for the unstructured mesh. In the present research both the type

of meshes are generated. The structured mesh was generated using the GridZ software of mesh generation whereas the unstructured mesh was generated in ICEM-CFD 14.5.

The important steps involved to generate the structured mesh are explained below:

3.4.1 Blocking

Blocking is a method of generating the structured volume grid across the geometry, thus creating grid domain for the geometry. In 2-D view the block seems to be like a rectangle while in 3-D it looks like hexahedra. In practice, the physical region is broken into pieces that each has a simple mapping from a rectangular grid. Depending on the shape, the structured grid topology is classified into three categories C, O, and H grid topology. Depending upon the geometry of the problem, the blocks are arranged. The number of blocks can vary till we get a best arrangement which would capture all the physics of the ow and bring out the best topology. In other words, the computational volume is divided into a set of non-overlapping, logically aligned rectangular blocks.

3.4.2 O-grid

O type mesh is ideally suited for circular or curved surfaces. An O-type grid has lines of points where the last point wraps around and meets the first point. Thus, the grid lines look like the letter 'O'. In O-type grids, the computational region is a solid square. In this case the system of co-ordinates is obtained by bending the square, sticking two opposite sides together and then deforming. This step of sticking the two opposite faces or edges is known as Mapping.

The reason why O-type grid is employed in this computational problem is because this type of grid can be best used to cover the maximum of the physics of the ow. As we know the ow over here in which we are interested is the internal flow and the region where the maximum effect of the flow can be seen is the inner walls of the inlet and outlet of the intake. This O-type grid covers the wall of the inlet efficiently and can produce a better result. It can provide us with the boundary layer effects. To generate the O-grid in for the S-duct, multi-blocking is done. Here five blocks are generated to efficiently produce an O-grid.

3.4.3 Procedure for Structured mesh generation

The steps employed for the generation of mesh are being discussed in this section. To start with the meshing there is a need of geometry. The geometry can possibly be modeled in the meshing software due to the provision of CAD tools in the software or the geometry

can be modeled separately in some other CAD software and then it can be imported in the meshing software. The second approach was followed. GridZ software supports various formats of geometry file extensions. After being imported it was founded that only curves and Non-uniform Rational B-Spline (NURBS) surface was retrieved.

The next step was now to create the surface of the geometry. The Piecewise Bi-Linear Surface (PBLs) can be extracted from the NURBS by giving the values for the number of points for the number of points in X and Y direction. This generates one PBLs. The procedure is repeated to generate the other surface. The PBLs is splitted radially into two to simplify the things for the mapping purpose. The Piecewise Linear Curves (PLCs) are also generated at the boundaries of the geometry by picking up boundary points on the PBLs and then converting the PBLs points into PLCs. It is shown in Fig.3.3.

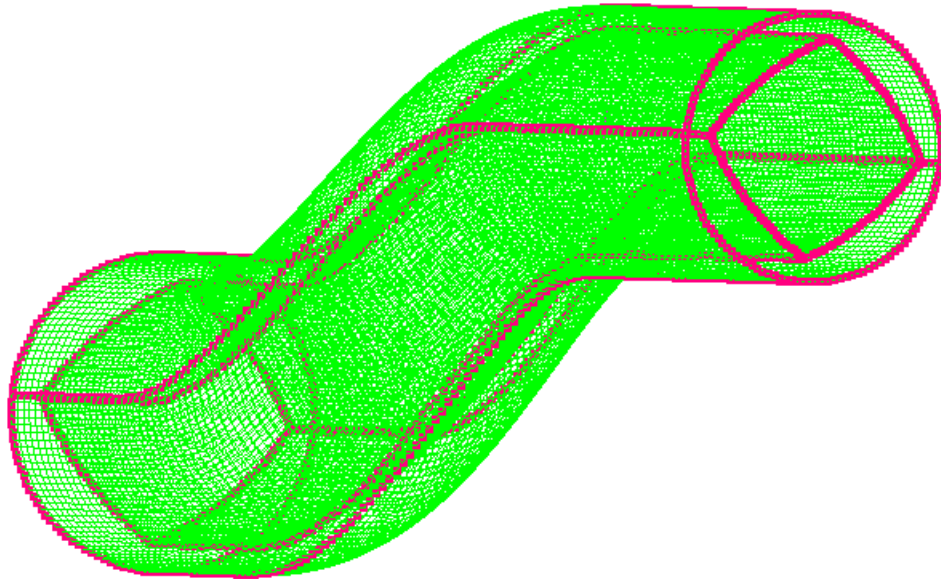


Figure 3.3: PBLs generated from NURB surface

Now, the next step is to perform blocking of the geometry. The blocks are to be so arranged that it can capture the complete flow and results into the grid that is best suited for the geometry. The desired grid in the present research is O-type grid. For this grid, five blocks are created as shown in the figure. Firstly a 2-D block is created and then with the help of option to generate block inside a block we generate another block. This causes the initial block to break into 5 small blocks. This sets the topology of the problem.

Now this 2-D block is mapped with the PLCs at the boundary of the surface. To map the inner block a virtual duct of same shape but of smaller size is created. This helps in better grid generation. After mapping of the edges the 2-D block is now converted to the

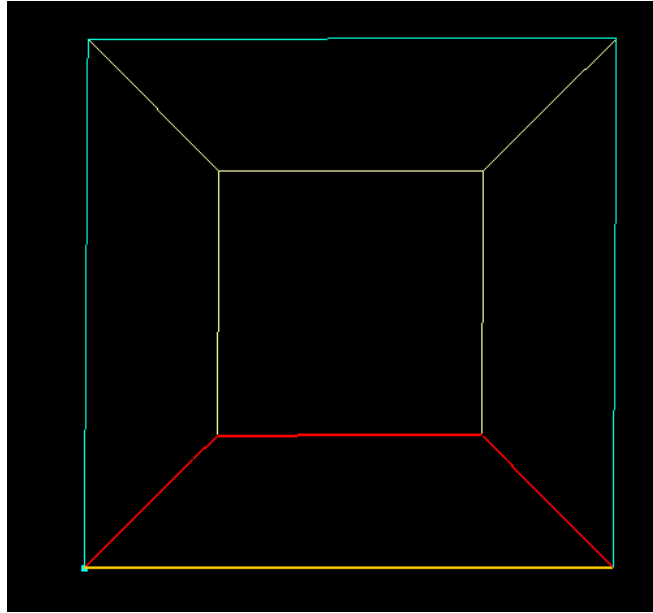


Figure 3.4: 2-D block generated for the geometry

3-D multi-block. Now the next step is to map the surface along with the surface of the 3-D multi-block. Mapping is simply done by projecting the block surface on the geometry surface. After the mapping step is done the volume mesh is generated. The Fig.3.5 shows the resulting structured grid.

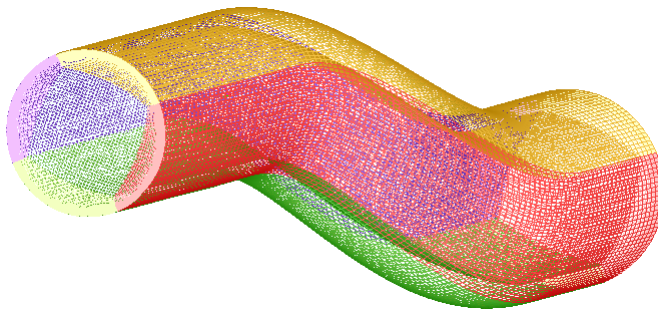


Figure 3.5: Structured mesh with O-grid

The volume mesh can be further improved by performing clustering operation to increase the number of element count near the inner wall of the elements. It is shown in Fig.3.6. The first wall element distance was calculated to be 0.018375 mm. The calculation was performed using NASA's Y^+ calculator. The calculation was done using $y^+ = 2$.

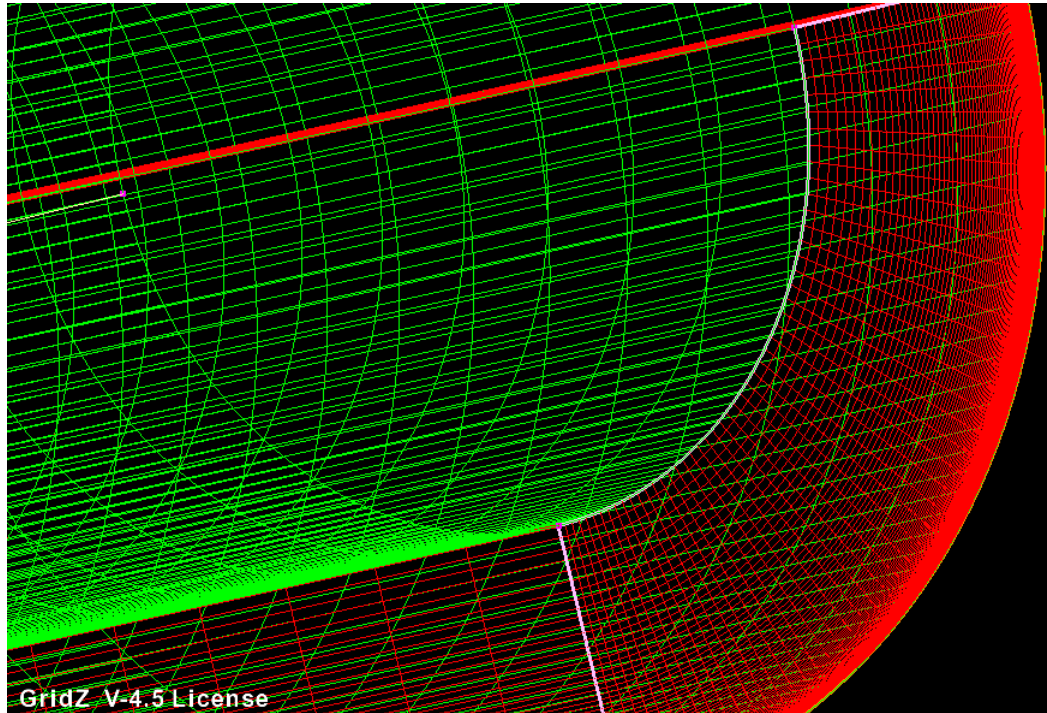
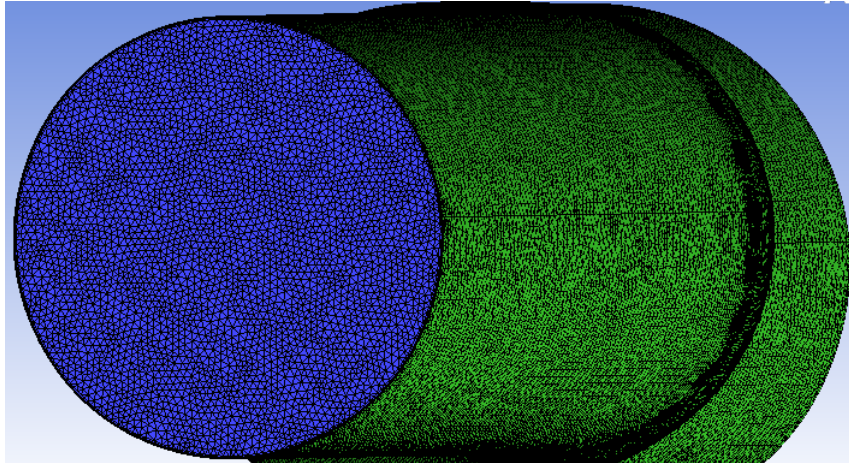


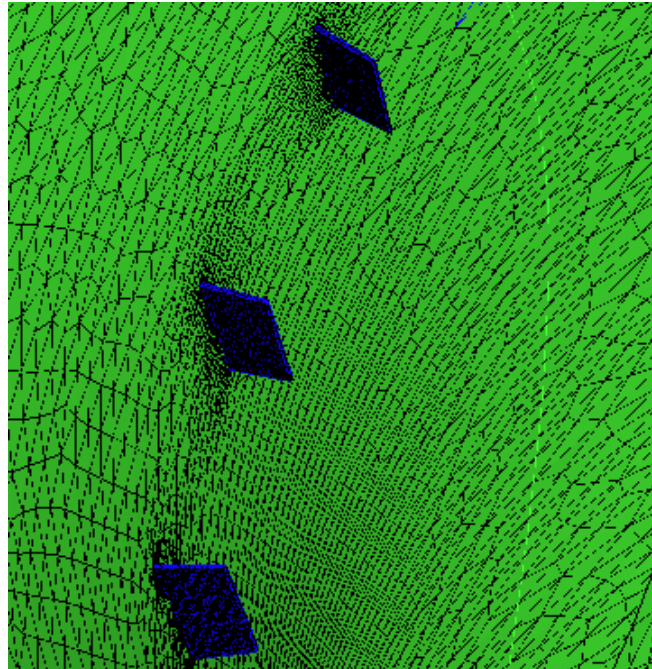
Figure 3.6: Final grid after clustering

3.4.4 Unstructured Mesh

The second mesh generated was the unstructured mesh as shown in Fig3.7a, Fig.3.7b. The unstructured mesh is the automatically generated mesh. Unstructured mesh was made in ICEM CFD-14.5. First, the surface mesh is generated for the air intake. The surface mesh consists of all the triangular elements. To capture the boundary effects of the wall, the prism layer is generated. The prism layer is generated in a product on ANSYS software known as T-GRID. A total of 15 layers of prism is generated so that the boundary layer effects can be captured effectively. After this the volume meshing is done. The tetrahedral elements are filled in using QUICK DELAUNAY technique. The quality of mesh was kept to be more than 0.25.



(a) Volume mesh with prism layer



(b) Mesh near vane-effectors

Figure 3.7: Unstructured mesh on S-shape air-intake

3.5 Computational Procedure in CFD-ExpertLite

In this section of the chapter a brief about the computational procedure is explained. Before the computation was started the mesh was divided into 4 zones to reduce the computational cost. The flow solver is required to setup the problem. CFD Expert Lite is the solver being used for solving the problem. CFD Expert Lite is developed by ZEUS Numerix Pvt.

Ltd. The software imports the mesh file in CGNS format. CFD Expert Lite uses Reynolds Averaged Navier-Stokes Equation (RANS). The convective scheme employed is Second-order upwind scheme. Second-order scheme provides with more accurate results than first-order scheme. Another reason for choosing this scheme was that second-order upwind equation is used for the pressure-based approach. The pressure based approach is employed basically for the incompressible flows and mildly compressible flows.

For measuring and keeping the control over the turbulence in the flow, a turbulence model is used. There are different turbulence model used in the flow analysis depending on the flow type. The turbulence model used in this study is Spalart Allmaras (SA) turbulence model. The SA model is very useful in internal flows as it is efficient in capturing all the effects.

Another parameter to be chosen is the gradient scheme. The gradients are needed not only for constructing values of a scalar at the cell faces, but also for computing secondary diffusion terms and velocity derivatives. The Green-Gauss scheme is used as the gradient scheme. Another important parameter to set for the flow solving is the convergence criteria. The convergence criteria are necessary to check the residuals, relative solution changes and other indicators to make sure that the iterations converge. The model employed for convergence is the Gauss-Siedel method. The convergence criterion given is $1e-06$.

After every 500 iterations the solution file was saved. In order to observe the correct results and parameters the input controls and operational conditions should be defined correctly.

3.5.1 Discretization method

There are several discretization schemes that are available for steady and unsteady analysis. Some of the approaches used for discretizing are Finite Difference Method (FDM), Finite Volume Method and Finite Element Method (FEM). In the research Finite Volume Method (FVM) approach is used. In FVM, the values are calculated at discrete places on a meshed geometry. The volume integral in Partial Differential Equation (PDE) is converted to the surface integral using the divergence theorem. The values are then calculated at the surface of each finite volume. The FVM method is a conservative method, as the mass entering the volume is equal to the mass leaving the volume. The mass, momentum and energy are conserved even on coarse grid. Another reason why FVM is used is that it does not limit the cell shape, it is very efficient and the iterative solvers for this method are well developed.

3.5.2 Boundary Conditions

The boundary conditions is a necessary step in setting up the problem in CFD for solving purpose. The boundary conditions are applied as shown in Fig.3.8 to obtain the actual

problem for the analysis purpose. The appropriate boundary for this present study are as follows:

- Inlet of Intake : The inlet is assumed to be a source from where the air comes in, therefore it is given Pressure Inflow boundary conditions.
- Outlet of Intake : The outlet of the intake is given the Outflow boundary condition.
- Wall of Intake : The walls of the intake is assumed to be viscous and to capture all the viscous effect and boundary layer, the wall is applied with the Viscous Wall boundary condition.
- The guide vanes : The guide vanes are also applied with the Viscous Wall boundary condition.

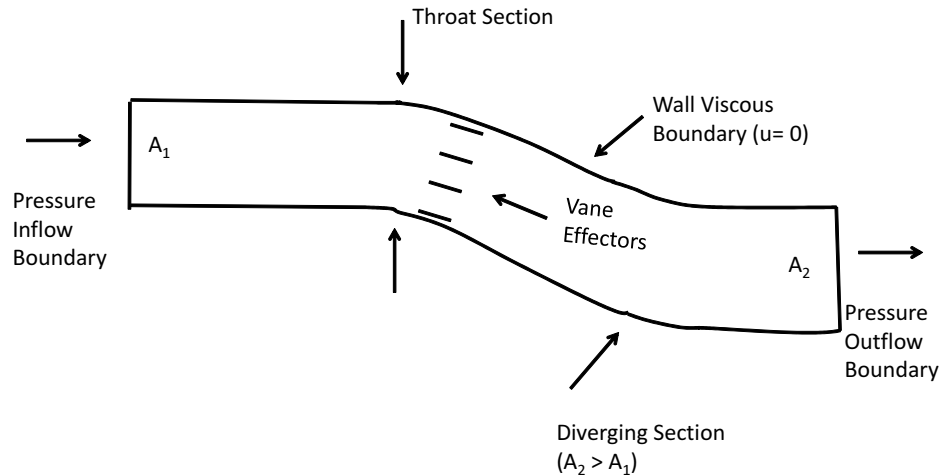


Figure 3.8: S-shape air-intake with boundary conditions

3.5.3 Initial Conditions

The initial conditions are certain guesses that are to be made just to initiate the flow to solve the problem. These guesses may be value of velocity, pressure, temperature. The initial conditions in this study varies for each case so it is discussed in detail in the next chapter.

Chapter 4

Results and Discussions

In this chapter the results obtained for the problem solved are shown. This chapter includes the grid independent study and the results obtained. The various losses and the phenomena occurring are quantified as well as their occurrence is discussed in detail. Both the qualitative as well as quantitative results are shown.

By applying the boundary conditions and initial conditions, a number of results were obtained. The initial conditions varied for each run. A total of 28 runs of the cases were done including the grid independent study. Each case was solved for 25000 iterations.

4.1 Initial Conditions

The initial conditions for each run are shown in the Table4.1. The Pressure inlet, Pressure outlet, Static temperature and Total temperature values are given as the initial conditions.

Table 4.1: Initial Conditions used for the solutions

Sr. No	Total Pressure TP (Pa)	Pressure inlet P_i (Pa)	Pressure outlet P_o (Pa)	Mach No.	Static Temperature (K)	Total Temperature (K)
1	101125.405	90569.52667	94871.9	0.4	278.1	287
2	101125.405	85250.84513	91769.2	0.5	273.33	287
3	101125.405	79282.951	88666.6	0.6	267.72	287
4	101125.405	72904.12192	85081.305	0.7	261.31	287
5	101125.405	66340.186	83495.51	0.8	254.43	287

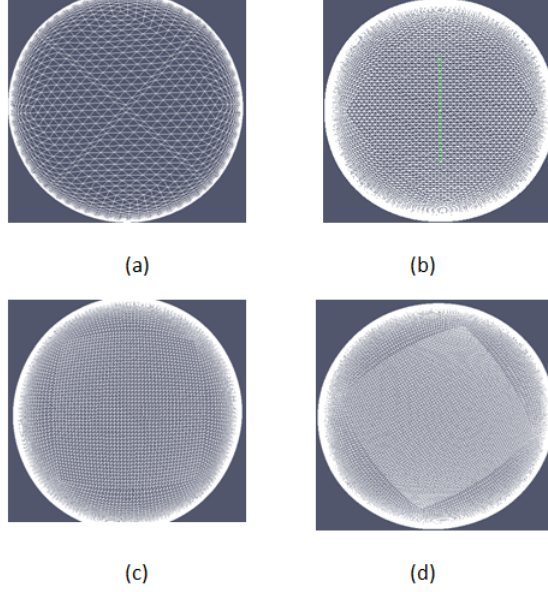


Figure 4.1: Different Grids: (a) Coarse grid, (b) Normal grid, (c) Fine grid, (d) Finest grid

4.2 Grid Independent Study

A total of four grids were used to perform this study. All the four grids are shown in the Fig.4.1a - Fig.4.1b. The coarser grid contained 92582 elements; normal grid contained 688842 grid elements while the fine and finest grid contained 969760 and 1394170 elements respectively. The grid independent study was performed for 0.6 mach at 0° angle of attack.

The $L - 1$ and $L - 2$ norm grid convergence criterion was chosen to perform the grid independent study. The total pressure at the engine face of the duct was calculated. It was seen that the $L - 1$ and $L - 2$ norm for the normal grid, fine grid and finest grid contained no significant changes therefore the normal grid was selected for further analysis.

4.2.1 Grid Convergence criteria

The grid independent study was carried out using the $L - 1$ and $L - 2$ norms. The norms are calculated for the total pressure values. The $L - 1$ and $L - 2$ norms are mathematically defined as:

$$L - 1 = \frac{\sum_{i=1}^{i=N} | P_N - P_{avg} |}{N} \quad (4.1)$$

$$L - 2 = \sqrt{\frac{(| P_N - P_{avg} |)^2}{N}} \quad (4.2)$$

where P_N is the total pressure at a particular face, P_{avg} is the free stream total pressure.

The grid convergence plot is shown in the Fig.4.2a-4.2b.

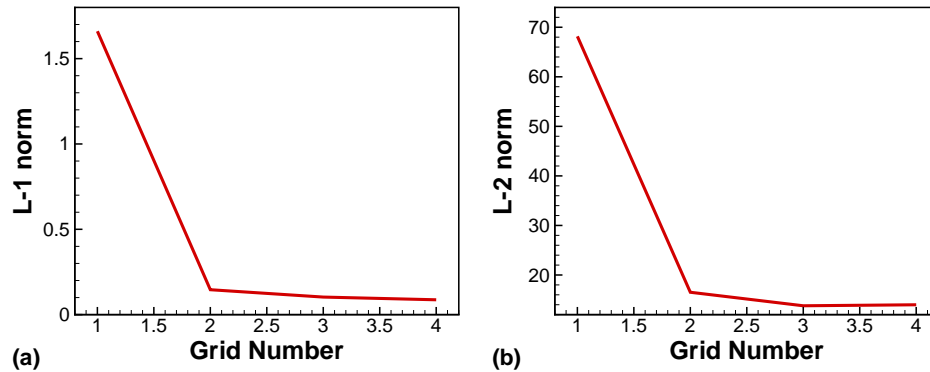


Figure 4.2: $L - 1$ and $L - 2$ norm grid convergence

From the above plots it can be seen that there is not much change in the $L - 1$ and $L - 2$ norms for the grid grid 2, 3 and 4. This implies that the best CFD results can be obtained by using normal grid. Therefore the grid number 2 i.e., normal grid is chosen for the further analysis.

4.3 Results obtained

The present study was divided into two parts, the first being for the S-shape air intake normal configuration i.e., without any geometrical modification while the other part was S-shape air-intake with geometrical modification i.e., with the vortex generator configuration.

4.3.1 S-shape air intake without vane-effectors

The S-shape air-intake normal geometry without the vane-effectors was analyzed for 5 different cases. As discussed in previous chapters, the parameters that define the performance of the S-shape air-intake are the total pressure recovery at the engine face, the total pressure loss, mach number variation. The air-intake was solved mainly for two AoAs, (i) Zero degree AoA and (ii) 10 degree AoA. 10 degree AoA is selected because it is the angle of airplane during the take-off phase of the aircraft. During the take-off time, the aircraft needs maximum amount of thrust. Therefore this is the time when the performance of the air-intake holds a key role of providing the engine with the pressurized air that is needed to generate the thrust.

The axi-symmetric profile of the total pressure is shown in Fig.4.3. The Fig.4.3a - 4.3e are for zero degree angle of attack whereas Fig.4.3f - 4.3j are for 10 degree AoA and these

are for 0.8, 0.7, 0.6, 0.5, 0.4 Mach number respectively. The profile of variation Fig.4.3a, 4.3f is similar which is for 0.8 throat Mach number. It can be seen that the total pressure is uniform till the first bend of the intake but as the flow goes downstream of the bend, the flow tends to separate in this region and this separation increases as it goes near the outlet of the intake. The region of flow separation is more for the Fig.4.3f, which is the 10° angle of attack case. The Fig.4.3 b,4.3g are for the 0.7 Mach number. The flow separation again starts from the intake bend region. The region of the flow separation is lesser than the 0.8 Mach case.

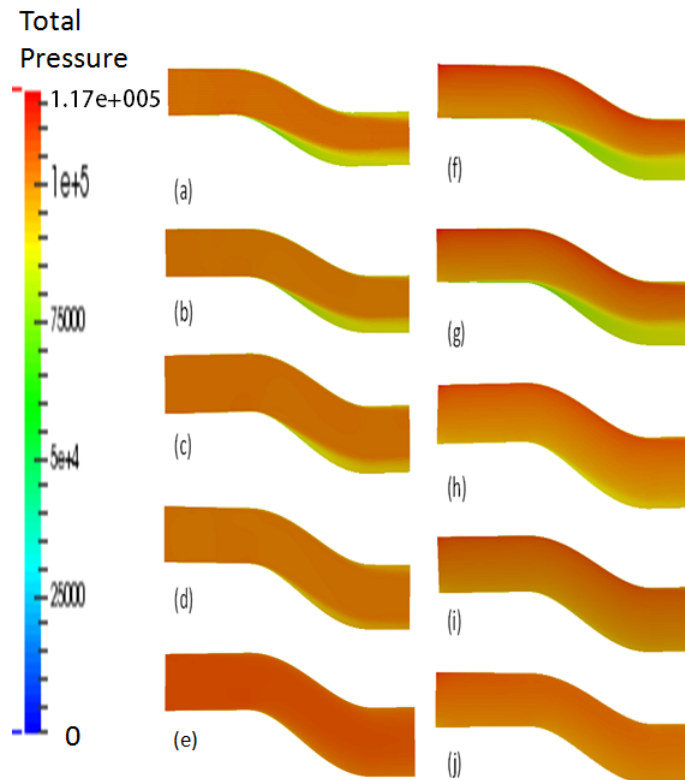


Figure 4.3: Axi-symmetric Total Pressure profile: (a) at 0° Angle of Attack (AoA) for Mach number 0.8, (b) at 0° AoA for Mach number 0.7, (c) at 0° AoA for Mach number 0.6, (d) at 0° AoA for Mach number 0.5, (e) at 10° AoA for Mach number 0.8, (f) at 10° AoA for Mach number 0.8, (g) at 10° AoA for Mach number 0.7, (h) at 10° AoA for Mach number 0.6, (i) at 10° AoA for Mach number 0.5, (j) at 10° AoA for Mach number 0.4.

There is no appreciable total pressure variation for the low mach number cases like Fig.4.3e, 4.3j. This is due to the fact that for the flow speed case, the flow gets enough time to develop inside the intake and no major pressure losses occur inside the intake. The total pressure variation intensity increases with the increase in mach number and also the

area of flow separation also increases with it. For 10^0 AoA cases it is seen that the flow separation region is more than the 0^0 AoA case. This means that for a high Mach number cases, there are more pressure losses and hence there would be less total pressure recovered. Since there is not much changes in the parameters for 0.4 Mach case therefore the 0.4 Mach case would be neglected for further study.

In the Fig.4.4 the Mach number profile of the air-intake for 0^0 and 10^0 AoA for the above mentioned Mach number cases is shown. Fig.4.4a and 4.4f is the 0.8 Mach case for 0^0 and 10^0 AoAs respectively. It can be clearly seen that the Mach number is maximum at the inlet of the air-intake and it tends to increase with the flow going forward till the throat. At the first bend of the intake, where the pressure losses occur, there is a sudden increase in the Mach number. This increase in Mach number complements the fact that there is pressure losses near that region. As the flow moves downstream of the first bend, the Mach number of the intake decrease. This is due to the fact that in this region, the flow separation is encountered which causes the Mach number to decrease. In Fig.4.4f, that is the 10^0 AoA case, the flow separation region is more. The flow separation region is more for the high Mach number case invariable of the AoA and the flow separation almost diminishes for the low Mach number cases. This is due to the fact that in the high speed Mach flow, the region after the first bend is untouched and untraveled but in the low Mach cases, the flow goes through the bends and develops in every part of the intake. Thus, in the low Mach cases the flow separation region is not present.

It is seen that as the mach number decreases the flow separation region decreases. This can be seen in the Fig.4.4c - 4.4j.

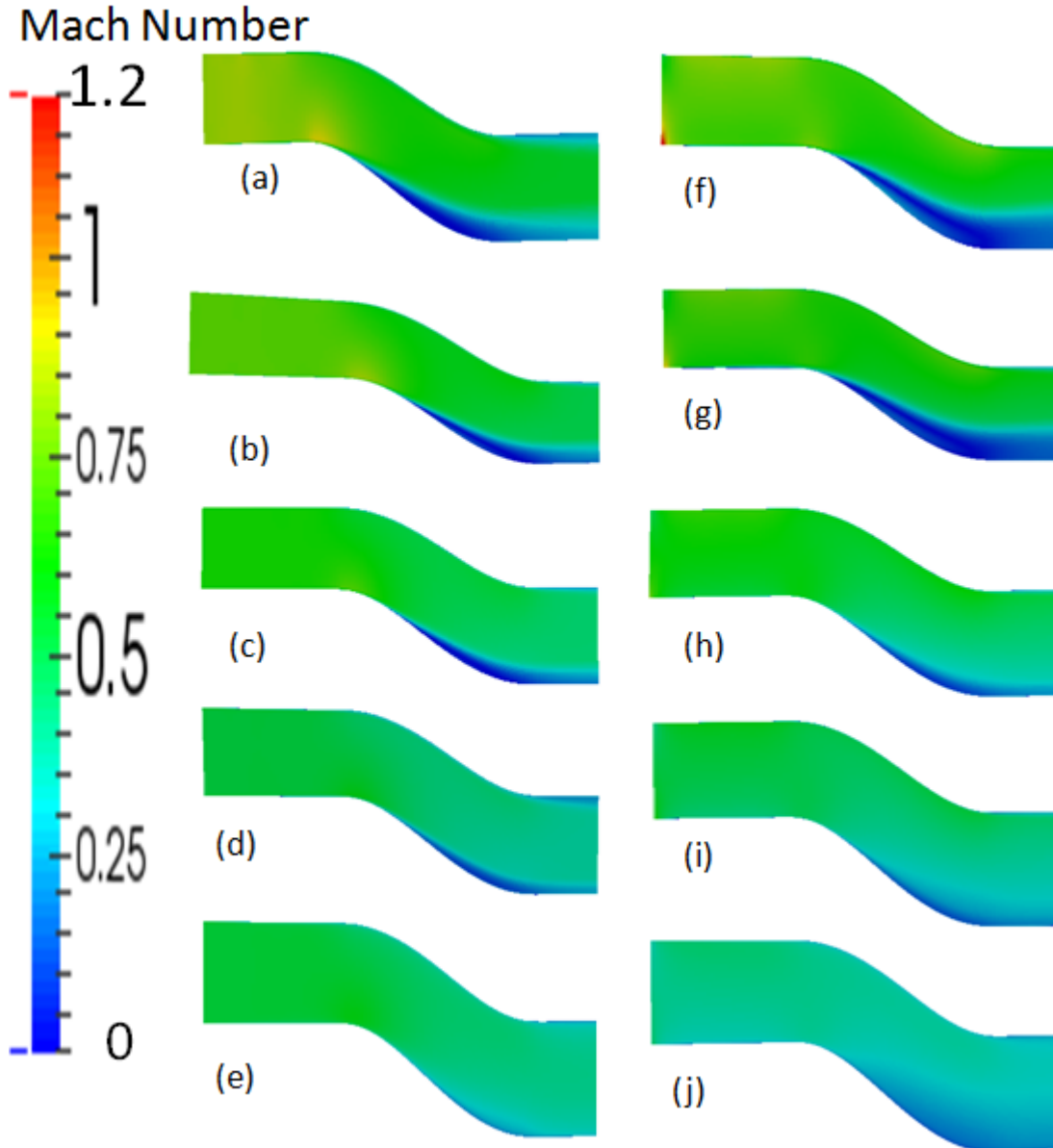


Figure 4.4: Axi-symmetric Mach number profile: (a) at 0° Angle of Attack (AOA) for Mach number 0.8 (b) at 0° AoA for Mach number 0.7, (c) at 0° AoA for Mach number 0.6, (d) at 0° AoA for Mach number 0.5, (e) at 10° AoA for Mach number 0.8, (f) at 10° AoA for Mach number 0.8, (g) at 10° AoA for Mach number 0.7, (h) at 10° AoA for Mach number 0.6, (i) at 10° AoA for Mach number 0.5, (j) at 10° AoA for Mach number 0.4.

4.3.2 Total Pressure Recovery

The parameter that defines the performance of the intake is the total pressure recovery. It defines how much the total pressure is recovered at the Aerodynamic Interface Plane (AIP) compared to the freestream total pressure. The total pressure was calculated at the engine

Table 4.2: Values of Total Pressure Recovery obtained for 0° and 10° AoA

Throat Mach Number	TPR at 0° AoA	TPR at 10° AoA
0.4	0.9882	0.987385
0.5	0.982387	0.980566
0.6	0.981562	0.97337
0.7	0.96624	0.959673
0.78	0.9637	0.95897

face or the outlet face of the air-intake. The values of Total Pressure Recovery obtained from the results is shown in Table4.2. The values of TPR for both the angle of attacks are provided and it is seen that the value of TPR decreases with the increase in Mach number.

It can be seen from the results that there is a pressure drop in the intake at the downstream of the bend. This flow separation leads to a drop in total pressure recovered at the AIP. It is to be noted that the values shown over here for the Total Pressure recovery at the aerodynamic interface plane and the value of throat mach number is area averaged values. From the above table it can also be seen that the TPR start to slightly decrease with the increase in angle of attack for the same value of throat mach number. The Total Pressure Recovery plot for without guide-vane configuration is shown in Fig.4.5. The profile of the two plots is almost same though the values does not match. Hence showing that the TPR value is decreasing with the increase in AOA. The total pressure recovery for both the plots decreases with the increase in Mach number. The concern over here could be that the TPR for high Mach case i.e., 0.8 and 0.7, are not producing a high amount of TPR. The effort is made to increase the value by making certain geometrical modifications. This is studied in the next section.

From the Fig. 4.6, the total pressure at the engine face is shown. The profile for each case is same. The darkest region is near the center of the intake. The figure also shows that the maximum total pressure area increases as the Mach number decreases.

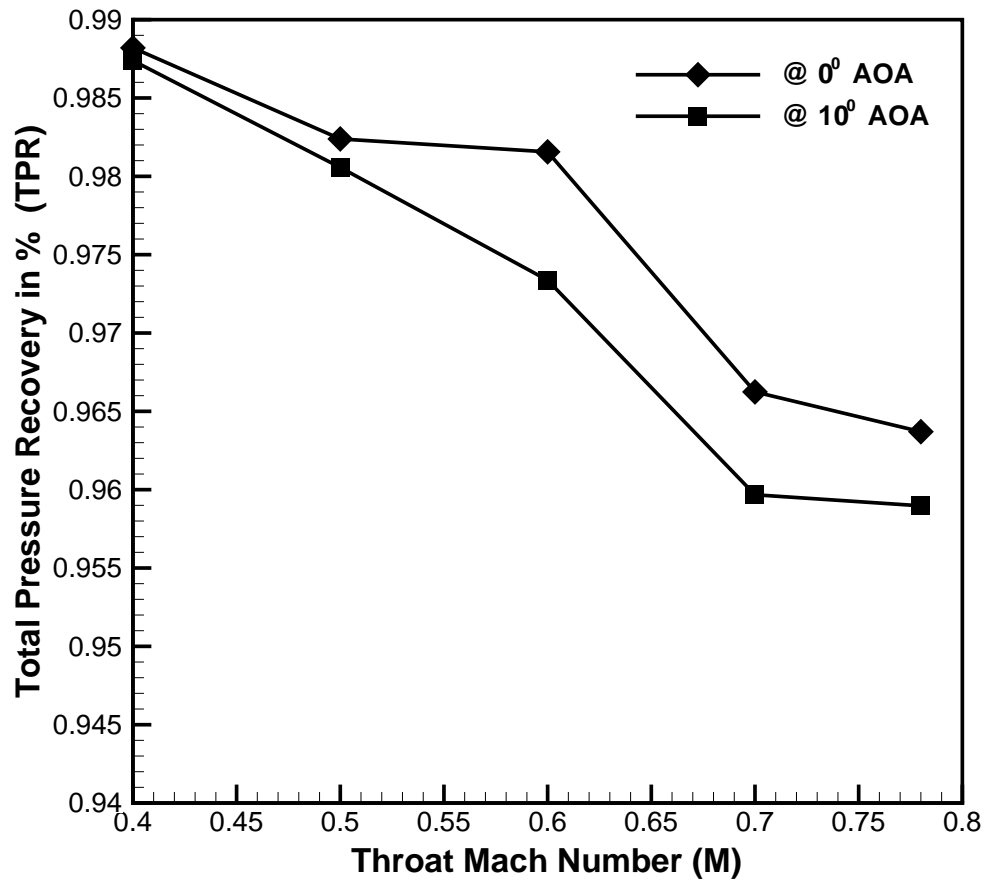


Figure 4.5: Total Pressure Recovery Plot

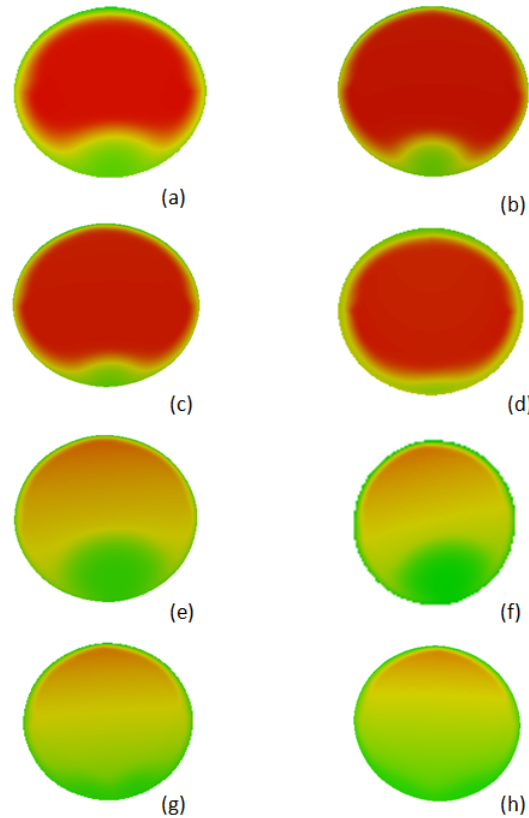


Figure 4.6: Total Pressure recovery at AIP or engine face for: (a) 0° AoA and 0.8 Mach number, (b) 0° AoA and 0.7 Mach number, (c) 0° AoA and 0.6 Mach number, (d) 0° AoA and 0.5 Mach number, (e) 10° AoA and 0.8 Mach number, (f) 10° AoA and 0.7 Mach number, (g) 10° AoA and 0.6 Mach number, (h) 10° AoA and 0.5 Mach number, (i) 10° AoA and 0.5 Mach number.

From the above Fig.4.6 it is clearly seen that the total pressure at the engine face increases with the decrease in Mach number. The total pressure profile as obtained at the engine face is shown in the above figure. The total pressure recovery can be improved by using certain devices. In the present study, an attempt has been made to improve the total pressure recovery by installing the vane-effectors that work as a vortex generator.

4.3.3 S-shape air-intake with vane-effectors

The second part of this chapter is to show the results of flow inside the S-shape air-intake with the vane effectors installed within it. The vane effectors are installed inside the duct to minimize the total pressure loss. The vanes are installed at the three angles 0° , 8° , 16° . The same boundary conditions and inputs were applied to perform the analysis.

The total pressure and Mach number are the major parameters that can define the flow type inside the air-intake. From the ideal intake earlier theories, it is known that the vane-

effector configuration that works as the vortex generator helps the intake to achieve the flow closest to the ideal intake. In an ideal intake the flow should develop near the throat and at the bend there should be minimum pressure losses and as it flow pass the bend, the flow should gradually decelerate so as to increase the pressure and also to recover the maximum pressure at the engine face.

The total pressure axisymmetric profile for the guide vane is shown in the Fig. 4.4 at different Mach numbers. There is a major change in higher Mach numbers therefore the cases for 0.8 and 0.7 are shown over here. Fig.4.7a, 4.7c and 4.7e is the axi-symmetric total pressure profile for 0.8 Mach number for 0° , 8° and 16° vane-effector angles whereas Fig.4.7b, 4.7d and 4.7f shows the axi-symmetric total pressure profile for 0.7 Mach number for 0° , 8° and 16° vane effector angles. Due to the AoA of the air-intake, there is a huge total pressure change at the inlet of the air-intake. After the flow is developed it can be clearly seen that the major area where the problem of the flow separation and pressure drop was occurring is getting diminished. In Fig.4.7e and 4.7f, the problem region at the first bend can not be seen and is almost removed. The angle of incidence of the vane-effectors for these two cases is 16° and this configuration of vane-effector works efficiently, thereby decreasing the eddies in flow by removing flow separation region and pressure loss region at the bend and increasing the overall total pressure at the AIP or the engine face.

From the Fig.4.7c and 4.7d it can be clearly seen that the 8° angle of incidence configuration of the vane effectors also removes the eddies region but not completely, only partially. The total pressure recovered at the AIP is therefore less than the total pressure recovered for the 16° configuration. The region of flow separation is also worked on and there is a considerable decrease in the area of that region. In Fig. 4.7a and 4.7b there is no difference in the flow and problem region. It is similar to the without vane configuration. The flow separation region as well as pressure drop region is clearly seen and there is no much change in the flow.

From the mach number point of comparison for all the cases it is seen that the losses are comparatively more for 0.8 Mach than the 0.7 Mach cases. The intensity of losses increases with the increase in mach number.

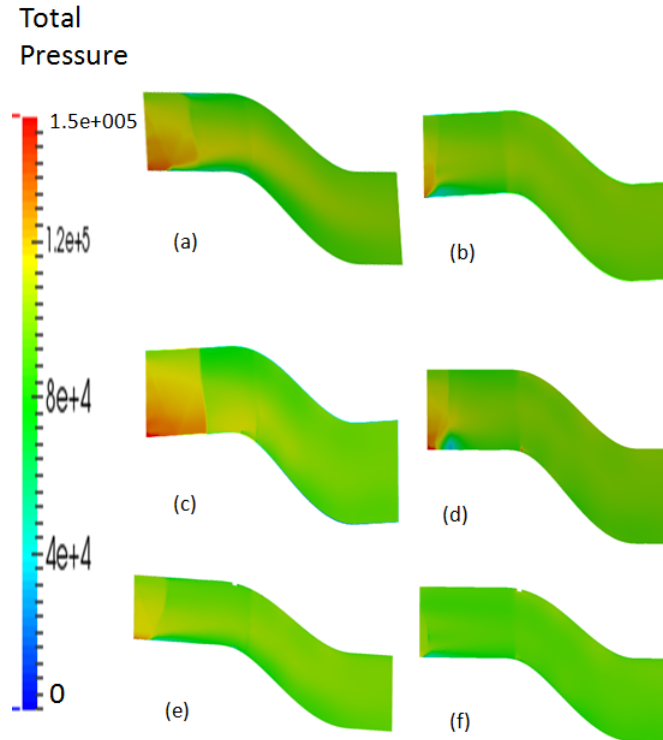


Figure 4.7: Axi-symmetric Total Pressure profile: (a) for 10° intake AoA and 16° vane effector angle for 0.8 Mach number, (b) for 10° intake AoA and 16° vane effector angle for 0.7 Mach number, (c) for 10° intake AoA and 8° vane effector angle for 0.8 Mach number, (d) for 10° intake AoA and 8° vane effector angle for 0.7 Mach number, (e) for 10° intake AoA and 0° vane effector angle for 0.8 mach, (f) for 10° intake AoA and 0° vane effector for 0.7 mach.

Fig.4.8 shows the axi-symmetric view of the Mach number profile for different vane effector configurations. Fig.4.8a and Fig.4.8b is the Mach number profile for the Zero degree vane effector configuration. From the figure it is very much clear that the flow separation at the downstream of the first bend region is very strong and it is similar to the without vane configuration. The eddies are though less for the 0.7 Mach case and the flow is much smoother for this case.

For the 8° vane-effector configuration Fig.4.7c, and Fig.4.7d, the flow separation region is delayed and the intensity of the flow separation decreases compared to 0° case. Initially the Mach number is high due to the angle of attack but as the flow tends to develop, it begins to decrease the flow as studied in the theory in the previous chapters. The flow is decelerated gradually and the flow separation region also tends to decrease. The case for 0.7 Mach is much smoother compared to 0.8, also the region of flow separation is also smoother and lesser.

Fig.4.7e and Fig.4.8f is for the 16° vane-effector. For both the cases the ideal air-intake

theory is followed, that is, the flow is gradually decelerated downstream of the bend. It can also be seen that the air-intake flow separation region is considerably reduced and the flow is very much uniform past this region.

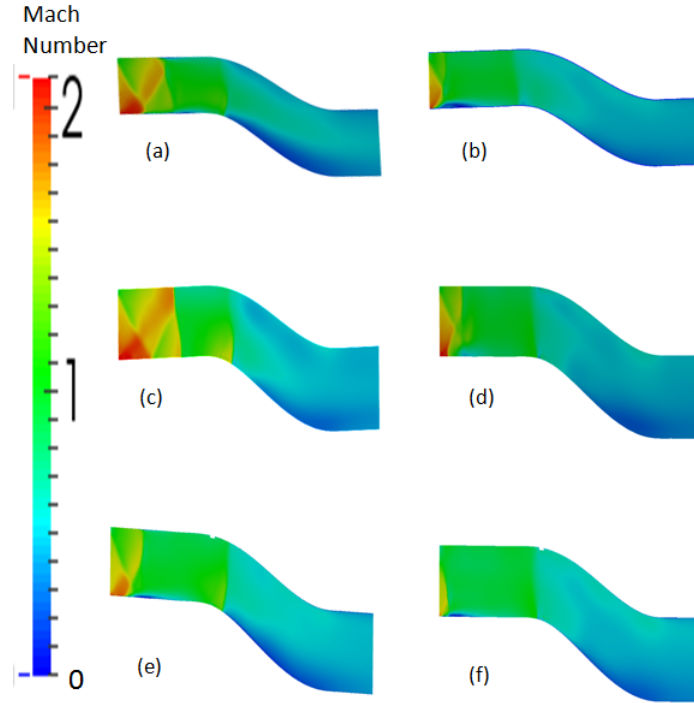


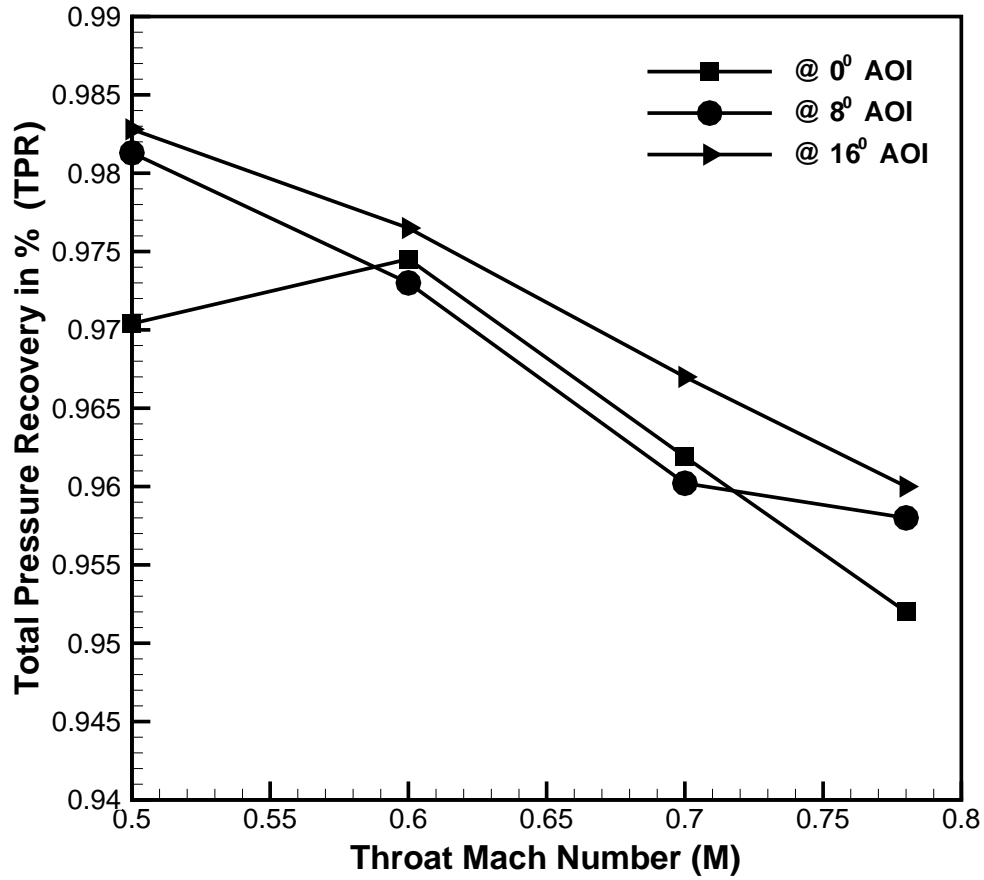
Figure 4.8: Axi-symmetric Mach Number profile: (a) for 10° intake AoA and 16° vane effector angle for 0.8 Mach number, (b) for 10° intake AoA and 16° vane effector angle for 0.7 Mach number, (c) for 10° intake AoA and 8° vane effector angle for 0.8 Mach number, (d) for 10° intake AoA and 8° vane effector angle for 0.7 Mach number, (e) for 10° intake AoA and 0° vane effector angle for 0.8 mach, (f) for 10° intake AoA and 0° vane effector for 0.7 mach.

4.3.4 Total Pressure Recovery

The total pressure recovery as obtained for the vane-effector configurations for different angle of incidence of vane-effectors are discussed in this section. The three different angles are 0° , 8° , 16° . The Table4.3 shows the TPR values for all the angle of incidence. It is seen that the TPR values have increased from the without vane configuration. The value for 16° is maximum for all the cases and it decreases as the angle of incidence of the vane decreases. The value of TPR for 0.5 mach case is maximum for all the three angles. The profile for all the curves is the same and is shown in the Fig.4.9.

Table 4.3: Total Pressure Recovery for different vane-effector configurations

Throat Mach Number	0°	8°	16°
0.5	0.9704	0.9813	0.9828
0.6	0.974518	0.973	0.9765
0.7	0.961897	0.96021	0.967
0.78	0.952	0.958	0.96

Figure 4.9: Total Pressure Recovery with vane-effectors at different angles for 10° AoA

Chapter 5

Conclusion and Future Scope

5.1 Conclusion

The CFD analysis of the S-shape air-intake was performed for two angle of attacks i.e. 0° and 10° and for two geometries i.e. a normal plane S-shape air-intake geometry and with the guide vane at different incident angles. Some of the important nature of the flow in the S-shape intake was studied throughout the study. The flow was visualized throughout the duct and it was seen that the flow inside an S-shape intake consists of a number of eddies. These eddies constitutes of high pressure losses at the bend, flow separation region downstream of the bend. This flow separation causes the total pressure recovered at the engine face to decrease. It was seen that the total pressure recovered at the engine face depends on the throat mach number. The total pressure recovery decreases with the increases in mach number. It was minimum for 0.78 Mach and maximum for 0.4 Mach case. For the plane intake geometry, the maximum pressure drop was obtained at the bend of the intake.

An attempt was made to improve the total pressure recovery by applying certain geometrical modifications. The vane-effector configuration was done for three angles. It was seen that the flow inside the intake changed with the change in geometry. The flow changed with the increase in angle of incidence of vane-effectors. The flow was closer to the ideal intake for 16° angle of incidence, as the flow separation minimized and the pressure loss region also reduced. These losses increased with decrease in angle of incidence. The total pressure recovered at the engine face was improved for the geometrical modification cases. The total pressure recovery was maximum for 16° and decreased gradually for 8° and 0° .

5.2 Future Scope

The flow inside an intake is a complex problem and therefore there is lot more that can be analyzed and studied.

- The grid independent study can be performed for the second configuration i.e, for the vane-effector geometry.
- The whole case can be solved for different turbulence models.

Bibliography

- [1] Abdellatif,O.E., Abd Rabbo,M.B., and Shahin, I.M., "Computational study of center line turning angle effect on the turbulent flow through a diffusing S-duct using large eddy simulation", Baulra University.
- [2] Abrahamsen, P.E.H., Petterson Reif, B.A., Sactran, L., and Fossdal, J.B., "Air intake studies : experimental measurements and computaional modelling", Published in RTO MP-5, 1998.
- [1] Anand, R.B., Singh, S.N., and Ra, L., "Effect of swirl on the flow characteristics of S-shaped diffusing duct",Indian journal of engineering and material sciences, 15, 317-325, Aug, 2008.
- [3] Biswas, A.K., Raman, A.K., Mullick, A.N., and Majumdar, B., "A numerical analysis of flow development through a constant are S-Duct", IPCSIT, 33, 2012.
- [4] Fiola, C.J., "Numerical simulation of separated and secondary flows in diffusing S-ducts for air breathing propulsion", Electronic thesis and Dissertation, 1168,2013.
- [5] Mathis, R., Duke, D., Kitsois, V., and Soria, J., "Flow control in S-shaped air intake using Zero-Net-Mass-Flow" , 16th Australian Fluid Mechanics Conference, Dec. 2007.
- [6] Menzies, R., "Computational investigation of flows in diffusing S-shaped intakes", Acta polytenica, 41, 4-5, 2001.
- [7] Singh, S.N., Seshadri, V., Chandel, S., and Gaikwad, M., "Analysis of the improvement in performance characteristics of S-shaped rectangular diffuser by momentum injection using CFD, Engineering application of computational fluid mechanics, 3, 109-122, 2009.
- [8] Wellborn, S.R., Okiishi, T.H., " A study of compressible flow through a diffusing S-duct", NASA Technical memorandum 106411, Dec 1993.
- [9] Wenzong, X., Rongwei, R., "A ventral divertless high offset S-shaped inlet at transonic speed", Chinese journal of aeronautics, 2008.

- [10] Wu, Y. L., Ng, E.Y.K., Wong, K., "Numerical study of swirl ow in F-5E intake with subsonic speed", *Mathematical and computer modelling*, 48 (2008) 447- 467.

Appendix A

Flow inside an S-shape air-intake without Vane-effectors

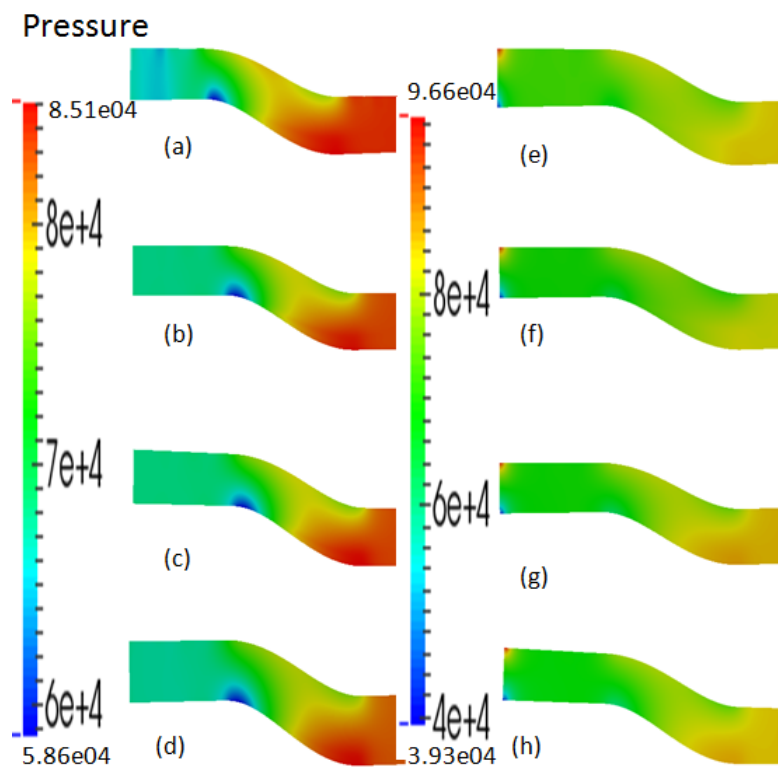


Figure A.1: Axi-symmetric profile of Static pressure variation for (a) Mach number 0.8 at 0° AoA, (b) Mach number 0.7 at 0° AoA, (c) Mach number 0.6 at 0° AoA, (d) Mach number 0.5 at 0° AoA, (e) Mach number 0.8 at 10° AoA, (f) Mach number 0.7 at 10° AoA, (g) Mach number 0.6 at 10° AoA, (h) Mach number 0.5 at 10° AoA

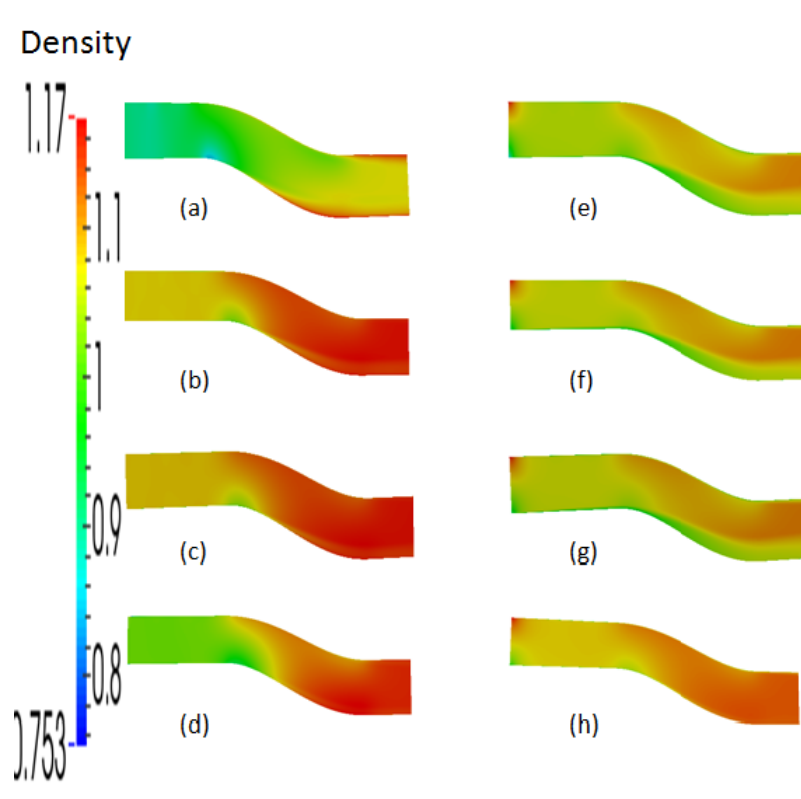


Figure A.2: Axi-symmetric profile of Density variation for (a) Mach number 0.8 at 0° AoA, (b) Mach number 0.7 at 0° AoA, (c) Mach number 0.6 at 0° AoA, (d) Mach number 0.5 at 0° AoA, (e) Mach number 0.8 at 10° AoA, (f) Mach number 0.7 at 10° AoA, (g) Mach number 0.6 at 10° AoA, (h) Mach number 0.5 at 10° AoA

Appendix B

Flow inside an S-shape intake with Vane effectors

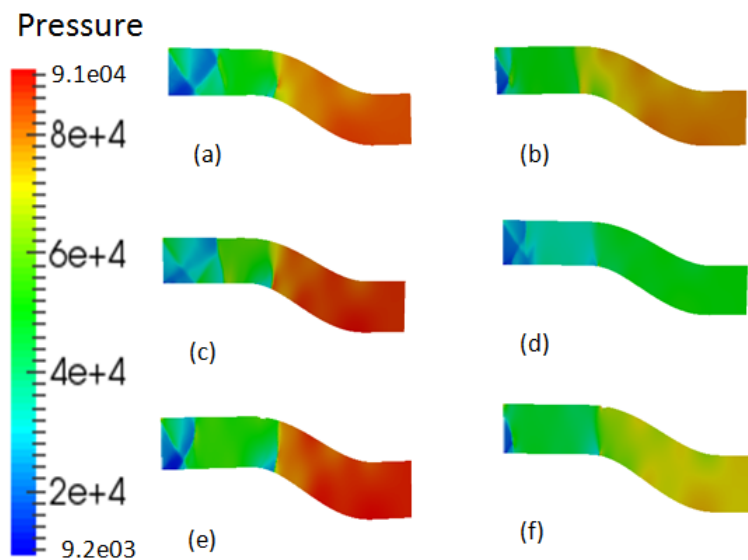


Figure B.1: Axi-symmetric Static Pressure variation profile for 10° AoA (a) Mach number 0.8 at 16° angle of incidence of vane effector, (b) Mach number 0.7 at 16° angle of incidence of vane effector, (c) Mach number 0.8 at 8° angle of incidence of vane effector, (d) Mach number 0.7 at 8° angle of incidence of vane effector, (e) Mach number 0.8 at 0° angle of incidence of vane effector, (f) Mach number 0.7 at 0° angle of incidence of vane effector.

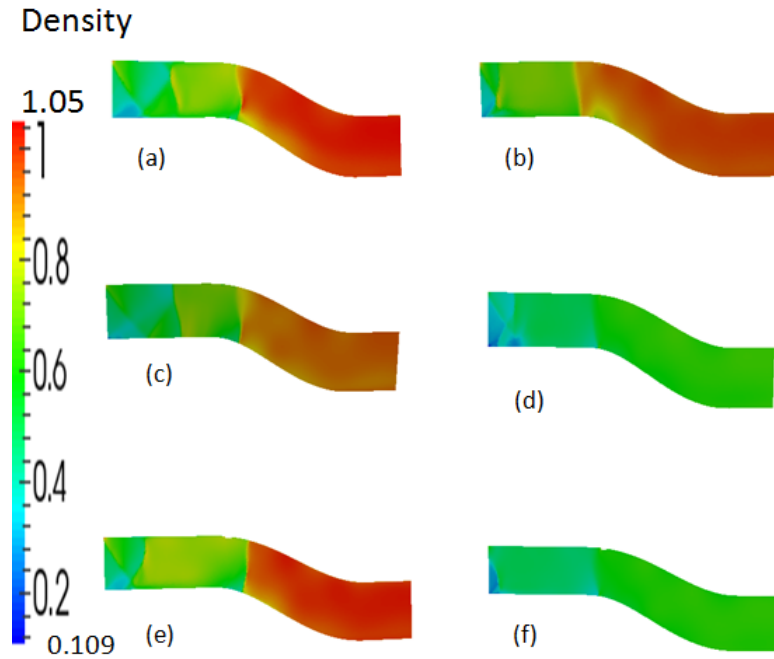


Figure B.2: Axi-symmetric Density variation profile for 10° AoA (a) Mach number 0.8 at 16° angle of incidence of vane effector, (b) Mach number 0.7 at 16° angle of incidence of vane effector, (c) Mach number 0.8 at 8° angle of incidence of vane effector, (d) Mach number 0.7 at 8° angle of incidence of vane effector, (e) Mach number 0.8 at 0° angle of incidence of vane effector, (f) Mach number 0.7 at 0° angle of incidence of vane effector.